Geoderma 459 (2025) 117349

Contents lists available at ScienceDirect

Geoderma

journal homepage: www.elsevier.com/locate/geoderma

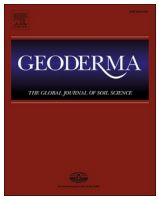

# Root traits of different wheat cultivars influence soil structure: an X-ray computed tomography and root morphology study

Bartolo Giuseppe Dimattia [a], Angela Righi [a,b], Matteo Bettuzzi [c], John Koestel [d], Maria Pia Morigi [c], Rosa Brancaccio [c,f], Silvio Salvi [a], Maria C. Hernandez-Soriano [e], Marco Bittelli [a,*]

[a] Department of Agricultural and Food Sciences, University of Bologna, Viale Fanin, 44, 40125 Bologna, Italy
[b] Department of Agronomy, Food, Natural Resources, Animals and Environment – DAFNAE, University of Padova, Viale Dell'Università 16, 35020 Legnaro, PD, Italy
[c] Department of Physics and Astronomy, "Augusto Righi", University of Bologna, Viale Berti Pichat 6/2, 40127 Bologna, Italy
[d] Soil Quality and Soil Use, Agroscope, Reckenholzstrasse 191, Zürich CH-8046, Switzerland
[e] John Innes Centre, Norwich Research Park, Norwich NR4 7UH, United Kingdom
[f] Department of Physics and Earth Science, University of Ferrara, via Saragat 1, 44121 Ferrara, Italy

ARTICLE INFO

Handling Editor: Yvan Capowiez

*Keywords:*
Soil morphology
X-ray computed tomography
Wheat cultivars
Root traits

ABSTRACT

Plant roots play a fundamental role in maintaining soil health. Although a broad range of root traits have been reported, few studies have attempted to link root morphology with soil structure. Here, we used shovelomics to characterize the root morphology of a wheat cultivar (Paragon), and two landraces (Senatore-Cappelli, and Watkins238), and advanced soil pore and root network X-ray computed tomography to assess their impact on soil morphology at cylinder and aggregate scales. Bare soil was analyzed as a control. Minkowski functionals and percolation theory parameters were computed to characterize soil pore network morphology. Bioporosity at the cylinder scale was significantly different for all cultivars compared to the bare soil. Bare soil presented the largest structural pore volume and the smallest biopore volume, this suggesting rapid degradation of biopores. At the cylinder scale, biopore characteristics were significantly different between Senatore-Cappelli and Watkins238, with Senatore-Cappelli exhibiting more pores with diameters >1 mm. The parameters from percolation theory revealed notable differences between the rhizospheric and bare soil samples. We found significant differences between genotypes, finding statistically significant correlations among root morphology parameters and pore network geometry.

Total imaged porosity and total root volume were limited descriptors of the effect of roots on soil structure, which is better quantified by pore network connectivity measurements. Our findings confirm previous studies on the relationship between root traits and soil properties and highlight the potential of our experimental approach to explore how different genotypes may influence soil morphology, paving the way for future applications in plant phenotyping.

## 1. Introduction

Soil structure, defined as the spatial arrangement of soil particles and pores, is a fundamental parameter for soil quality (Dexter, 1988, Young et al., 2001). Soil pores provide a habitat for microorganisms and play a major role in infiltration, root growth and carbon turnover (Kravchenko and Guber, 2017). Soil structure is also directly linked to soil hydraulic properties (e.g. water retention and hydraulic conductivity) that determine the availability of water for plants and soil microbial communities and key processes such as gas exchange, thermal properties, soil organic matter transformations, nutrient dynamics and root penetration (Horn et al., 1994, Bittelli et al., 2015).

A vast number of soil processes depend indeed on its complex structure, but its characterization and quantification remain challenging due to: (a) the various hierarchies of scales ranging from very small pores, to aggregates and large cavities and (b) the multitude of complex shapes and geometries that are difficult to interpret. The interactions between plant roots and soil add additional levels of complexity. Plant

* Corresponding author.
*E-mail address:* marco.bittelli@unibo.it (M. Bittelli).

https://doi.org/10.1016/j.geoderma.2025.117349
Received 12 April 2025; Accepted 14 May 2025
Available online 27 May 2025

roots can significantly affect soil physical structure through the formation and activity of biopores, modification of the density and distribution of soil pores, and by affecting the soil's capacity to retain water. Previous research has indicated that different root phenotypes can significantly impact soil structure by forming pore spaces, influencing water infiltration, and facilitating aggregate formation (De La Fuente Cantó et al., 2020). Considering that crop production claims nearly one third of the world land (Ritchie and Roser, 2019), it is crucial to introduce root traits in crop systems that can improve soil structure parameters such as porosity and aggregation (Lal, 2015). Reducing the detrimental impact of crop production on agricultural land remains a key goal of policies such as the European Green Deal (Montanarella and Panagos, 2021). Therefore, immediate measures to reverse current trends in soil degradation and restore and support soil productivity require strategies that preserve soil structure (Lal, 2009). Wheat landraces are a valuable source of genetic diversity (Cheng et al., 2024) for the introduction of root traits in modern cultivars that can be beneficial for soil structure (Marone et al., 2021). Accordingly, crops that improve soil physical properties have become a major breeding target (Lynch, 2022). Particularly, identifying root traits in wheat cultivars that can enhance soil productivity and breeding them into commercial elite cultivars is a key goal for improving crop yields (Ober et al., 2021). Wheat is a target crop since it plays a key role in global food security due to its nutritional and economic value (Shiferaw et al., 2013). Therefore, identifying root traits in wheat that enhance soil structure can advance our capability to support sustainable and profitable wheat production. Current collections of wheat cultivars such as the A.E. Watkins238 landrace collection (Wingen et al., 2014, Cheng et al., 2024) and the Global Durum Wheat Panel (Mazzucotelli et al., 2020) are untapped sources of diversity to identify root traits that have been lost through breeding and modern agricultural practices and breed them into modern cultivars. Root traits such as root depth, root length, xylem diameter and root hairs can improve water use efficiency by enhancing soil structure (Wasson et al., 2012). Root traits associated to the relationship between soil structure and soil biota play a key role in reshaping and modifying plant performance and crucial soil biological processes such as nutrient cycling (Brussaard, 2012; Rabot et al., 2018). Importantly, it is well established that root systems, particularly fine roots, induce specific structural changes by increasing pore space heterogenization and promoting aggregate coalescence (Carminati et al., 2010, Mooney et al., 2012, Bodner et al., 2014) Overall, the root morphology and processes associated with the rhizosphere significantly contribute to structural dynamics and function through bioturbation (Meysman et al., 2006; Lucas et al., 2019a).

According to Pagliai and Vignozzi (2002), the most relevant approach to assessing soil structural properties is the characterization of the pore system. For this reason, and for the ability to measure further and more detailed morphological properties, X-ray computed tomography (CT) is now increasingly used to assess soil and root structure (Bardgett et al., 2014 Young et al., 2022). In recent years, several studies have explored the impact of roots on morphological assessment of soil structure, primarily focusing on comparing how different ecosystems and cultivation methods shape soil pore structure (Kuka et al., 2013; Burr-Hersey et al., 2020; Kan et al., 2023).

While extensive research has explored the reciprocal relationship between soil structure and root growth (Tracy et al., 2012; Dal Ferro et al., 2014; Mawodza et al., 2020; Giuliani et al., 2024), investigations into the effects of root growth on soil structure have primarily relied on soil water retention curves (Angers and Caron, 1998; Logsdon, 2013; Bodner et al., 2014; Scholl et al., 2014). However, methods that are based on the capillary bundle model (Childs and Collis-George, 1948) often lack the ability to provide a comprehensive morphological characterization of the pore space due to oversimplification of the soil geometry (Hunt et al., 2013). This critique becomes even more pertinent when considering biopores, which possess distinct geometries and topologies (Leue et al., 2019).

Helliwell et al. (2019) investigated the impact of different plant species and their interaction with different soil types while Phalempin et al. (2021) assessed bulk density in the rhizosphere for different soil conditions. Here, for the first time we examined the impact of the genetic diversity of three wheat cultivars with different root morphological features on soil structure. The cultivars were selected from a preliminary screening of root morphology on a set of 20 wheat cultivars. We quantified the impact of the contrasting root morphology of an elite cultivar (Paragon) and two landraces (Watkins238 and Senatore-Cappelli, hereafter referred to as Senatore) grown in a field trial on key soil morphological and topological properties, both in soil cores and soil aggregates. Root crown morphology was determined using shovelomics and broken roots (Trachsel et al., 2011).

The results presented in this paper advance our understanding of the relevance of root traits to support soil structure.

## 2. Materials and methods

### 2.1. Field trial

The field trial was conducted at the experimental farm of the University of Bologna in Cadriano (44°3255 N, 11°2452 E, 26 m a.s.l.), located in the Pianura Padana valley, in northern Italy. The area is characterized by a subhumid climate with a mean annual temperature of 12.8 °C and an average annual precipitation of 924 mm. The soil is classified as loam, consisting of 11.6 % clay, 52.8 % silt, and 35.6 % sand, with a bulk density between 1.1 and 1.3 g/cm$^3$.

Following a preliminary screening of the root morphology of 20 wheat cultivars and varieties, the following were selected based on contrasting root morphology: a bread wheat landrace (Watkins238), the bread cultivar Paragon, and the durum wheat landrace Senatore-Cappelli. The selection aimed at maximizing diversity in root architecture while also considering species differences and their breeding history of each genetic diversity. We intentionally selected: (i) an elite bread wheat variety with a robust root system, (ii) a durum wheat landrace characterized by a highly branched root system, (iii) a bread wheat landrace with fewer but slightly thicker roots. This selection ensures a broad spectrum of root system variability. Additionally, by incorporating both elite and landrace varieties from different species, we aim to capture variability not only in root traits but also in their evolutionary and breeding trajectories. For further clarity, we have included a PCA plot (available in the Supplementary material) that visually represents the divergence among these genotypes.

The three selected cultivars are phylogenetically distinct and sourced from two collections of tetraploids (Maccaferri et al., 2016, Mazzucotelli et al., 2020) and hexaploidy wheat (Wingen et al., 2014). These cultivars were sown in 6 × 1-m (6 m$^2$) plots for the first time on November 26, 2022, on soil that had not undergone any tillage in the previous two years. Each cultivar was grown in three different plots according to a randomized experimental design. The field was not cultivated and not tilled for two years to reduce the potential effect of other crops or tillage on soil structure. The plants were subjected to two rounds of nitrogen fertilization at a rate of 24 kg/ha: the first on February 13, 2023, during the tillering stage, and the second on April 17, 2023, during the stem elongation stage. Wheat was harvested on June 10th, 2023.

### 2.2. Sample collection

Undisturbed soil cores were collected in October 2023 using an Eijkelkamp soil sampler. The samples were collected between rows and at the center of each plot between residual wheat plants. After harvesting the wheat in June 2023, no other crop was cultivated, and no tillage was performed. Additionally, samples of bare soil were collected outside the rhizosphere plots as a control. The bare soil had been grown by weeds prior to October 2022 but been bare after that date. Sampling was conducted at a soil depth of 10 cm (corresponding to the bottom of the

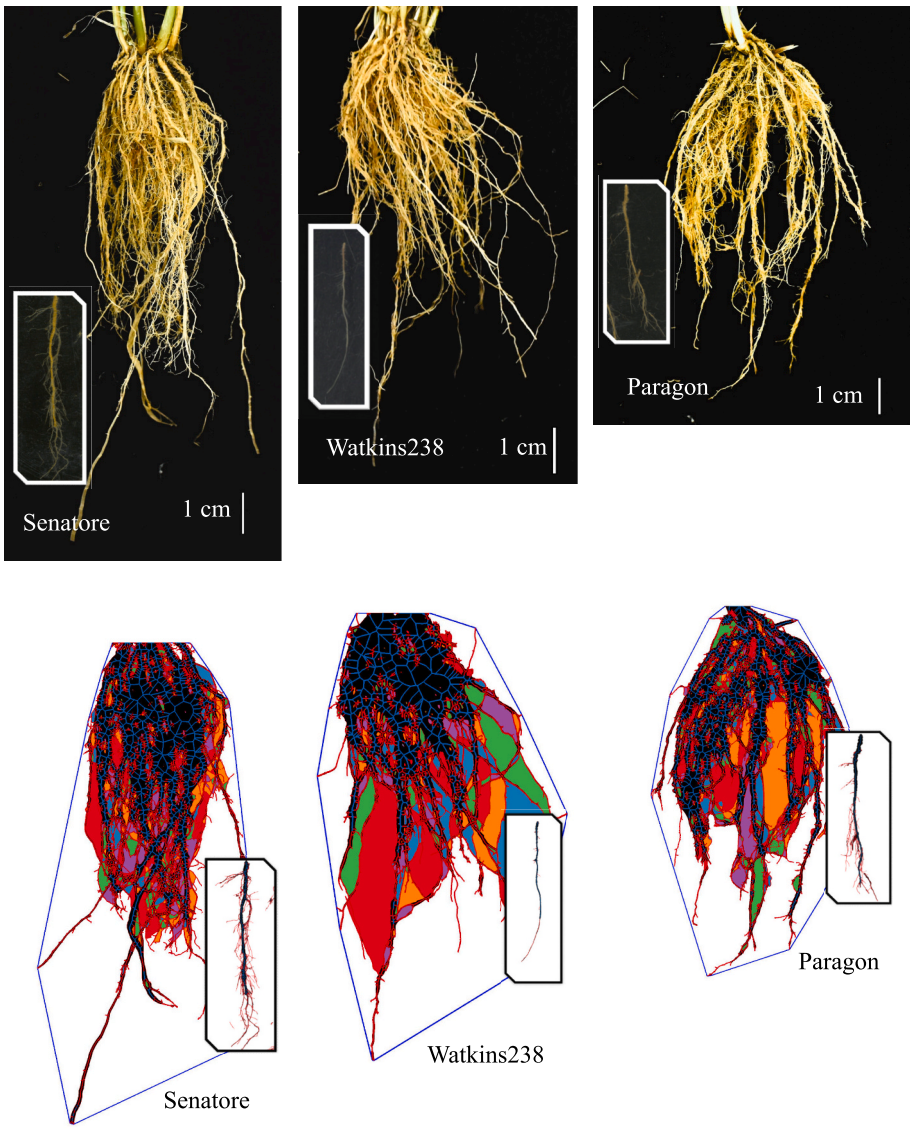


**Fig. 1.** Photos of the root crowns of the three wheat cultivars (top) and the corresponding image analysis output from RhizoVision Explorer (bottom). In the RhizoVision Explorer output, root segments are color-coded based on their diameter: red lines represent Range 1 roots (0–1.6 mm), while blue lines represent Range 2 roots (>1.6 mm). The colored regions within the roots indicate fragmented root morphological patterns, highlighting structural variations. The outer blue contour delineates the convex hull area, which represents the minimum convex boundary enclosing the root system.

sampler), using an aluminum cylinder, which was selected due to its suitability for X-ray analysis (Koestel et al., 2018). The cylinder used had an internal diameter of 8 cm, a height of 5 cm and had a wall thickness of 2 mm. Three undisturbed bare soil samples were collected as controls (bare soil) and three for each cultivar.

The samples were preserved at a constant temperature of 18 °C and covered with aluminum foil to prevent soil shrinkage. Any excess soil protruding from the aluminum cylinder was removed. Following the X-ray scanning of the undisturbed soil cylinder, sub-samples of soil aggregates were collected and used for scanning at a higher resolution for the aggregate soil structure analysis. X-ray analysis was therefore performed on the whole soil cylinder and on aggregates, as detailed below.

### *2.2.1. Root phenotyping*

Root phenotyping of the selected cultivars was conducted on May 27, 2023, during the flowering stage, to ensure complete root development using shovelomics (Trachsel et al., 2011). A 40 cm long and 30 cm deep soil block was excavated with a shovel. The analysis was performed for three plants for each plot (cultivars), for a total of eighteen plants per cultivar. After washing the roots of the excavated plants, three plants were selected for phenotyping as representative of the plants collected per plot regarding average number of tillers, plant height and root system size. Plants with visible malformations, signs of disease, or damaged root systems were excluded. Shovelomics was performed using two methods: whole root (crown) and broken root image analysis (Trachsel et al., 2011).

Whole roots were photographed with a black matte background (Fig. 1). The plants were positioned 80 cm above the ground, with the camera placed 80 cm away from the black matte background and 80 cm above the ground surface. To provide a comprehensive view of the root system morphology in three dimensions, each plant was photographed first from a frontal view, then rotated 90 degrees, and photographed again. The values of the root traits were therefore an average of both two-dimensional (2-D) images (Liu et al., 2021).

Broken roots were also imaged following the whole root analysis. The seminal and nodal roots were separated from the main culm and arranged in a plexiglass tank placed over an Epson Expression 12000XL Pro scanner, filled with 1.5 L of water to prevent overlapping. The main

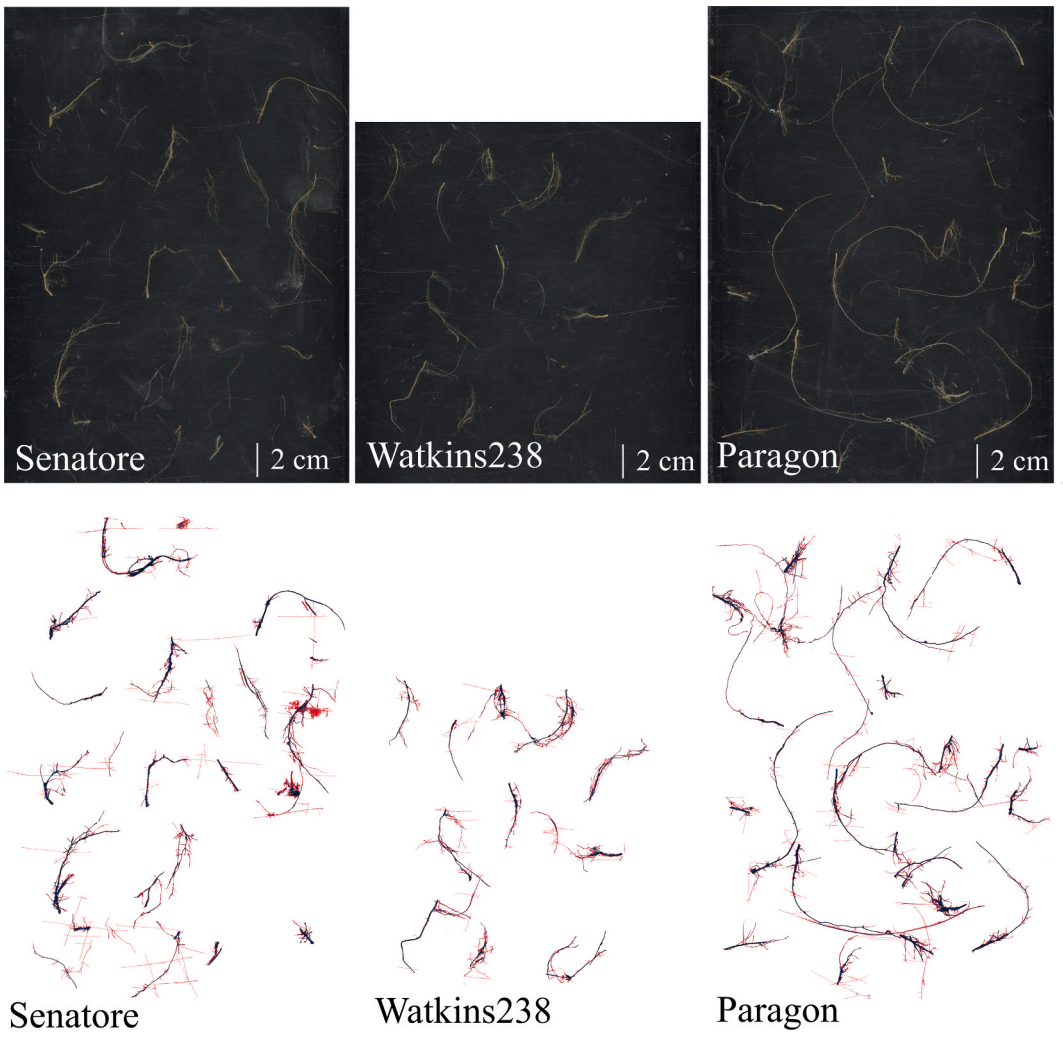


**Fig. 2.** Photos of the dissected main culm of the three wheat cultivars (top) and the corresponding image analysis output from RhizoVision Explorer (bottom). In the RhizoVision Explorer output, root segments are color-coded based on their diameter: red lines represent Range 1 roots (0–0.5 mm), while blue lines represent Range 2 roots (>0.5 mm).

culm of the plant was identified based on its greater height than the other tillering culms. A reference marker was included, and the tank was covered with a matte black lid to reduce reflections and interference. Images were captured at a minimum resolution of 600 DPI (Fig. 2). To maintain image quality, the water was replaced every 10 samples.

*2.2.2. Root image analysis*

Root image analysis was performed using RhizoVision Explorer software for both the whole-root and broken-root methods (Seethepalli et al., 2021). This software has been extensively validated and utilized in previous research within the shovelomics framework (Bucksch et al., 2014; Le Marié et al., 2019; Seethepalli et al., 2021; Xu et al., 2022; Prince et al., 2022; Weihs et al., 2024). RhizoVision Explorer provides two distinct analytical modalities: "whole-root analysis," used to evaluate entire root system images, and "broken-root analysis," which examines root fragments obtained after sectioning.

For whole-root analysis, focusing specifically on crown images, an image threshold value of 170 was employed to achieve precise segmentation of the root structures. Pixel-to-millimeter conversion was accomplished using a known-length reference scale and the Fiji software (Schindelin et al., 2012), with a resulting pixel-to-mm ratio of 8.6 pixels/mm, equivalent to an approximate resolution of 116 μm per pixel. Thirty-two root traits were derived from whole-root images, among which six key traits were selected due to their relevance to the study objectives and support in the literature: network area, convex hull area, root holes, shallow angle frequency, and steep angle frequency (Trachsel et al., 2011; Maccaferri et al., 2016; Ober et al., 2021). The parameter initially named "root holes," indicative of disconnected root segments, was renamed for clarity as "fragmented root morphological pattern". This trait, determined by analyzing the inverted segmented images (Seethepalli et al., 2021), quantifies the branching degree and structural complexity of the root system. Higher values for this trait denote greater complexity and branching, potentially reflecting enhanced soil exploration capability, nutrient and water uptake efficiency, and improved soil aggregation capacity (Balashov and Bazzoffi, 2003).

For the broken-root image analysis, thresholding levels were set differently to enhance segmentation accuracy: 200 for fine roots and 170 for axial roots. Root diameters were categorized into two narrower classes: root diameter range 1 (0–0.5 mm) and root diameter range 2 (>0.5 mm), enabling a more precise assessment of detailed root topology. Pixel-to-millimeter conversion followed the identical approach as described for whole-root analysis, ensuring consistency between methods.

A total of twenty-two root traits were extracted from broken-root images. To facilitate direct comparison with the whole-root analysis, five critical traits were prioritized: number of root tips, root length in diameter range 1 (0–0.5 mm), root length in diameter range 2 (>0.5 mm), branching points, branching frequency, as well as average and

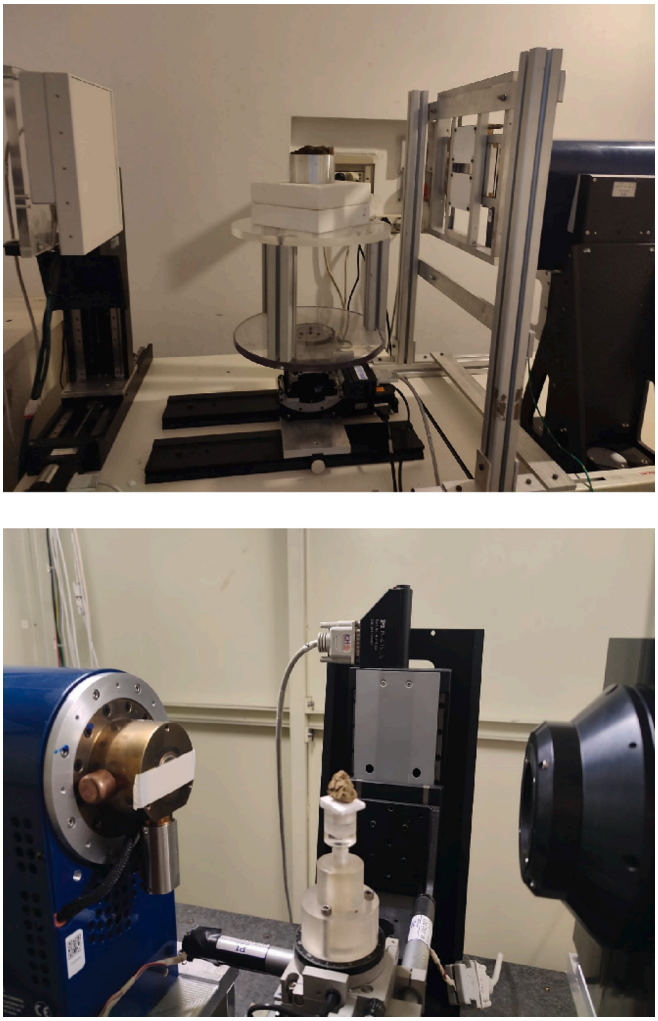

**Fig. 3.** Setup system with a soil sample on the rotating axis. In the upper picture the measurement of the cylinder sample and the in the lower picture one of the collected aggregates from each sample.

maximum root diameter. The total root length was computed by summing the root length of diameter range 1 and diameter range 2 classes.

The two analytical methods employed are complementary: whole-root analysis provides comprehensive information regarding overall root system architecture, whereas broken-root analysis offers detailed insights into finer structural and topological root characteristics. However, traits such as root tips, branching frequency, and branching points should be interpreted with caution, as they may be slightly overestimated due to background noise or limitations in feature detection inherent to the analysis software (RhizoVision Explorer).

### 2.3. X-ray scanning

X-ray images were taken with two different cone-beam X-ray CT systems at the Department of Physics and Astronomy at the University of Bologna. The X-ray scanning processes were controlled remotely by means of in-house proprietary software developed for research purposes (Zagaglia, 2012). Images of the undisturbed cylinders were collected using a PXS10-65 W MicroFocus X-ray tube (Thermo Kevex X-ray LLC) with a tungsten anode, a Varian PaxScan 2520D flat-panel detector and a Physik Instrumente M-038 PD1 precision rotary stage. The operating voltage was set to 130 kV, and the beam current was set to 240 μA. An optical lead filter of 0.3 mm was used to reduce beam-hardening effects. A total of 900 projections were acquired over a rotation of 360 degrees, and ideally, the number of projections should be the same as the number of horizontal pixels, which is 1500 in the detector. However, since the object did not occupy the entire field of view, 900 projections resulted in an optimal approximation. The exposure time per radiograph was adjusted to 250 ms, and the projection was averaged from 8 consecutive radiographs to reduce image noise. The voxel size was approximately 63 μm. We estimated the X-ray image resolution to be three times greater than this value, i.e., approximately 190 μm.

For the soil aggregates, a PXS10-65 W MicroFocus X-ray source was used in combination with a Photonic Science VHR 1:1 X ray camera and a Physik Instrumente M-037 precision rotary stage. Since the object size and the distance between the tube and the detector were significantly smaller than those of the ring sample, it was possible to work with a lower voltage, which we set to 110 kV and an electron current of 70 μA. We added an iron filter of 0.1 mm thickness. The exposure time per radiograph was set to 2 s. Again, we collected 900 projections over a rotation of 360 degrees, and each projection was averaged again from 8 consecutive radiographs. The voxel size was approximately 9 μm, resulting in an estimated image resolution of 27 μm. Fig. 3 illustrates the X-ray imaging systems for the cylinder and the aggregates collected from each measured cylinder.

The tomographic reconstruction software PARREC (Brancaccio et al., 2011) was used to filter the projections to remove imaging artifacts. This was performed in two steps. The first step was the application of a local threshold filter, using the local standard deviation for thresholding. Secondly, the projections were converted to sinograms and ring artifacts caused by malfunctioning detector pixels were corrected. Then the sinograms were re-converted to projections and a back-projection Feldkamp algorithm was used to reconstruct the sequence of frontal slices of each sample. Finally, 3D images were obtained by means of the rendering software VGStudio Max 2.0 by Volume Graphics.

### 2.4. Image processing

#### 2.4.1. Denoising

Digital images consistently contain noise to some extent, this being defined as casual brightness variation, i.e., that is not present in the original object. This can be due to measuring instruments, data transmission or quantization. Schlüter et al. (2014) reviewed the best denoising methods for micro tomography images and indicated that a nonlocal means filter is especially suitable for soil-like materials. This filter is based on the replacement of the gray level of a given pixel with an average of the gray levels of similar pixels, which allows overcoming the issues associated with the classical principle of denoising based on neighborhood values. As a 3-D implementation of a non-local means filter is not available as a Fiji plugin, we applied a 2-D non-local means filter (Buades et al., 2011) in all three different dimensions as described in Nitzbon et al. (2022). The smoothing factor was set to 1, and the noise standard deviation sigma was set to be auto estimated.

#### 2.4.2. Calibration and segmentation

To segment the images from each sample series, i.e., the cylinder and aggregate samples, with the same value, a calibration was performed beforehand. The following steps were carried out using the SoilJ plugin (Koestel, 2018). First, the 3-D cylinder outlines were delineated. Then, the gray values were rescaled to the 0.1-percentile of each cross-sectional histogram and the gray value of the aluminum wall. The rationale behind this approach is that the 0.1-percentile corresponds to air-filled pores (see Koestel et al., 2020). For the aggregates, calibration was performed by using values of the 10 and 60-percentiles since there was no aluminum wall to use as an upper reference. The 0.6 was found to correspond to the matrix gray value. After the gray-value calibration, joint histograms, i.e., a single representation of gray-values intensity distributions from all slices of all the scanned samples, were compiled from the cylinder and aggregate scale images, respectively. and used to compute threshold values with different methods: Otsu, Minimumn,

**Table 1**
Mean values of root traits for the three wheat cultivars. Mean values associated with different letters indicate statistically significant differences ($p < 0.05$, Tukey's test).

| Root trait | p_value[a] | Paragon | Senatore Cappelli | Watkins 238 |
|---|---|---|---|---|
| | *Whole root analysis* | | | |
| Network area ($mm^2$) | ** | 4435 ± 361[a] | 5667 ± 391[b] | 4145 ± 454[a] |
| Convex area ($mm^2$) | ** | 15002 ± 1460[a] | 16291 ± 2206[b] | 14714 ± 1659[a] |
| Shallow angle frequency | ns | 0.22 ± 0.02[a] | 0.24 ± 0.01[a] | 0.23 ± 0.01[a] |
| Steep angle frequency | ns | 0.51 ± 0.02[a] | 0.46 ± 0.01[a] | 0.48 ± 0.02[a] |
| Fragmenter root morphological pattern | * | 451 ± 27[a] | 637 ± 86[b] | 636 ± 75[a] |
| | *Broken root analysis* | | | |
| Root tips | *** | 894 ± 127[b] | 506 ± 60[b] | 237 ± 45[a] |
| Total root length (mm) | *** | 6086 ± 828[ab] | 3200 ± 416[b] | 1353 ± 322[a] |
| Root length diameter range 2 (mm) | *** | 1157 ± 100[b] | 546 ± 175[a] | 283 ± 42[a] |
| Root length diameter range 1 (mm) | *** | 4928 ± 734[b] | 2654 ± 743[a] | 1170 ± 249[a] |
| Branching points | *** | 3479 ± 612[ab] | 1447 ± 189[b] | 635 ± 165[a] |
| Branching frequency ($mm^{-1}$) | *** | 0.69 ± 0.08[b] | 0.35 ± 0.01[a] | 0.29 ± 0.03[a] |
| Max root diameter (mm) | ** | 1.93 ± 0.50[b] | 1.17 ± 0.13[a] | 1.19 ± 0.56[a] |
| Root diameter (mm) | *** | 0.93 ± 0.09[b] | 0.56 ± 0.01[a] | 0.60 ± 0.02[a] |

[a] ) p values of ANOVA genotypic effect, with *, ** or *** representing $p < 0.1$, $<0.05$ or $< 0.01$, respectively.

Isodata, Renyi Entropy, Maximum Entropy, Huang, Li and Yen (Prewitt and Mendelsohn, 1966; Ridler and Calvard, 1978; Otsu, 1979; Kapur et al., 1985; Huang and Wang, 1995; Yen et al., 1995). The gray value used as a threshold for segmentation was the average of all the global method thresholds listed before. Once the images were binarized into imaged pores, a morphological opening (erosion followed by dilation) of a cubic structural element of 2 voxels was performed. This approach allows for overcoming the fact that objects smaller than 3 voxels are likely to be noise.

#### 2.4.3. Biopore extraction

Pores of different sizes and shapes belong to two main categories: abiotic pores and biopores. Among the abiotic pores are textural pores which originate from the arrangement of primary particles (sand, silt, and clay), and affect soil structure at the macroscale, such as the typical formation of cracks in silty soil. Biopores are the result of biological activity; in particular, in the rhizosphere, they are the result of root exploration, which pushes mineral particles and organic substances aside (Lucas et al., 2019a). Once the root decomposes, the biopore persists as a tubular structure in soil. We used the workflow described by Lucas et al. (2019b) implemented in SoilJ to extract the biopores from the binarized images.

### 2.5. X-ray CT image analysis

To characterize the soil structure, four Minkowski functionals and three percolation theory parameters were computed from the binarized images for the total imaged porosity and the bioporosity, and at both cylinder and aggregate scale. The Minkowski functionals, or the quermass integral, are described as the "intrinsic volume" of an object and are valuable tools for describing soil structural properties since they are scale invariant (Vogel et al., 2010) and express information on the topology of the porous material through the Euler number (Renard and Allard, 2013; Armstrong et al., 2018). Negative values of the Euler number denote a higher number of redundant paths within pore-clusters than the number of isolated pore-clusters. Pore morphology and connectivity are also defined through the parameters obtained from percolation theory (Liu and Regenauer-Lieb, 2011; Koestel et al., 2020). The three parameters that best describe the connectivity of a system are the connection probability (Γ), which measures the likelihood of two random pore voxels being connected, and thus belong to the same cluster; the percolation threshold (PT), indicating the minimum porosity needed for a continuous pore network; and the critical diameter, representing the largest pore size that allows fluid flow through the soil. Thus, these parameters were computed to investigate soil morphology.

The first Minkowski functional, the phase volume fraction (M0), represents the most basic characteristic of porosity, i.e., its total volume. The second indicator, the surface area (M1), represents the area of the total imaged porosity, which is a relevant indicator of water adsorption and chemical exchanges between the solid and fluid phases. The third functional, the mean curvature (M2), is affected by the pore shape and is a relevant indicator of soil mechanical properties (Vogel et al., 2010). Finally, the fourth functional measures the total curvature. If it is divided by 4π, the Euler characteristic (M3) is obtained. The Euler characteristics is a topological property that carries information on the local connectivity of a porous medium (Renard and Allard, 2013). Negative values of the Euler number denote a higher number of redundant paths within pore-clusters than the number of isolated pore-clusters.

In the natural sciences, connectivity is also defined through the parameters obtained via the percolation theory paradigm (Liu and Regenauer-Lieb, 2011; Renard and Allard, 2013). Originally, percolation theory investigated at which porosity two opposite sides of an infinite domain become connected. Applied to soil science, it has been used to evaluate if an imaged soil pore-network contains a connected pore-cluster that spans from top to bottom surface of a soil sample (Jarvis et al., 2017). We used three parameters from percolation theory to quantify the pore network connectivity: the connection probability (Γ), the (apparent) percolation threshold (PT), and the critical pore diameter (CPD).

The connection probability is defined as the probability that two randomly chosen pore voxels in the region of interest (ROI) are connected (i.e., they belong to the same pore cluster). Its upper bound is 1 and it may asymptotically approximate 0. Larger values indicate better interconnected pore systems.

However, since the beneficial effect on total pore connectivity of a root system is given by an enhanced connectivity of the whole system itself, only the connectivity and Euler number of the whole pore system was discussed and not of the biopore system.

The apparent percolation threshold was determined using the method proposed in Liu and Regenauer-Lieb. (2011). It refers to the minimum porosity required for a continuous network of pores to form. Note that the apparent percolation threshold strongly depends on the image resolution, since it only expresses percolation properties for pores with diameters larger than the image resolution. Pores with smaller diameter may well percolate at lower porosities but are not resolved by the image data. A higher percolation threshold indicates that the gap needed to bridge for obtaining a pore connection from top to bottom of the ROI is larger. The critical pore diameter is only defined if at least one percolating pore cluster exists. Then it corresponds to the bottleneck in the pore connection from top to bottom, i.e., it is equivalent to the diameter of the largest sphere that could be moved from top to bottom through the pore system. In undisturbed soils, the square of the critical pore diameter is correlated with the saturated hydraulic conductivity (Koestel et al., 2018; Schlüter et al., 2020).

The labels for the morphological parameters for the cylinder and aggregate were chosen as follow: M0, M1, M2, M3, Γ and PT for the cylinder analysis and μM0, μM1, μM2, μM3, μΓ and μPT for the aggregate

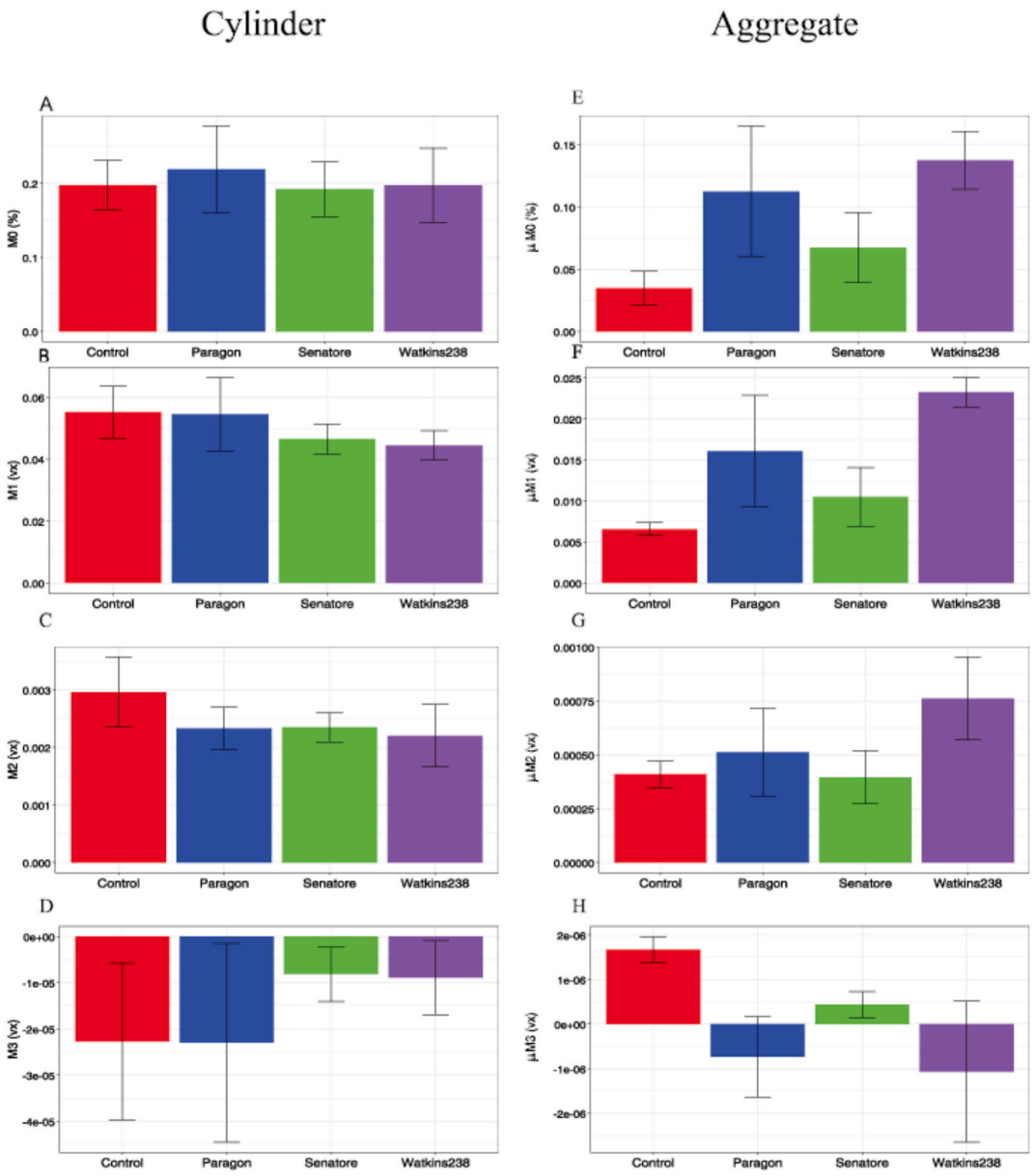


**Fig. 4.** Values of M0 (pore volume), M1 (surface area), M2 (mean curvature) and M3 (Euler number) for the bare (red bar) and rhizospheric soil from the three wheat cultivars (blue, green and purple bars) from the cylinder and the aggregate setups. The values are computed for the total imaged porosity.

sub samples.

The pore size distribution (PoSD) was also extracted from both rhizospheric samples with a thickness analysis of the pore space using the maximum inscribed sphere method using the software SoilJ (Koestel, 2018), to obtain a PoSD by attributing each pore voxel to its class diameter. Nonlinear regression models were used to quantify different continuous probability distributions. The best fit was obtained for an inverse Gamma distribution (Kahle and Stamey, 2017):

$$f(x;\alpha,\beta) = \frac{\beta^{\alpha}}{\Gamma(\alpha)}(1/x)^{\alpha+1}e^{-\beta/x}$$

where α is the shape factor, which is defined as $\alpha = 2 + \mu^2/\sigma^2$ and β is the scale factor, $\beta = \mu\,(\alpha - 1)$. Four parameters can be extracted from each inverse Gamma distribution: shape, scale, mean and variance (α, β, μ and $\sigma^2$). Two PoSD (Pore Size Distribution) curves were obtained for the different cultivars: one derived from the aggregate samples and the other from the ring samples. The first curve represents a pore diameter range from 0.03 to 0.7 mm, while the second curve covers the range from 0.19 mm to 2 mm. The two curves overlap at approximately 0.2 mm.

### 2.6. Statistical analysis

Firstly, we tested whether the parameters for normal distribution by using the Shapiro-Wilk test. For those parameters that did not adjust to normal distribution, a nonparametric Kruskal-Wallis test was used to assess differences among the cultivars and between the cultivars and the control for parameters that were normally distributed, Tukey's post-hoc analysis was performed to identify which cultivars primarily contributed to the significant differences. For non-normally distributed parameters, the Conover post-hoc test was used instead (Dinno, 2024). In the case of bioporosity the analysis was performed only on geometrical properties, i.e., the first three MF. Connectivity parameters were excluded because biopores can be linked by structural pores without a tubular shape, which the plugin cannot detect, and this would have led to misleading results.

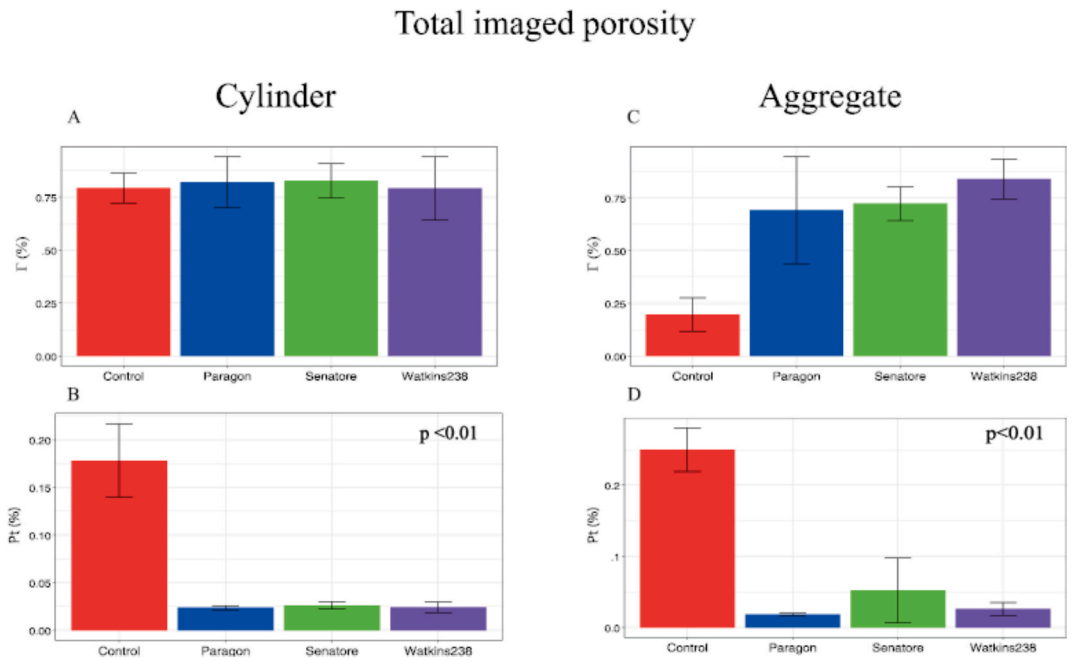


**Fig. 5.** Values of the connection probability Γ and the percolation threshold for the cylinder and the aggregate, for the control (red bar) and three cultivars (blue, green and purple bars). The values are computed for the total imaged porosity.

The PoSD curves, modeled as inverse Gamma functions, were compared using the Kolmogorov–Smirnov (KS) test.

The impact of the root traits of the cultivar and varieties on soil morphology was determined using an ANOVA and a Tukey post hoc analysis. To investigate the relationships between soil pore-network properties and root traits, linear regression models were used to evaluate all the interactions of the soil and root variables. The statistical analyses were performed using R software (RStudio Team, 2020). To analyze the effect of each root trait on the soil morphological parameters, data from the cultivars was combined. Since we wanted to explore the effects of root morphological traits on soil structure this analysis was conducted with the bioporosity parameters only. The analysis was conducted by using a mixed linear model (LMM) providing 96 combinations, where each root trait was analyzed in terms of its effect on the morphological parameters of the bioporosity alone.

## 3. Results and discussion

### 3.1. Root traits

The genotype Senatore-Cappelli exhibited a statistically significant bigger convex hull and network area compared to Paragon and Watkins238 ($p < 0.05$) (Table 1). There were no significant differences in the frequency of root angles among the cultivars ($p > 0.05$). The genotype Paragon exhibited significantly higher values of root tips, branching points, and total root length compared to Senatore Cappelli ($p < 0.05$). Watkins238 showed significantly lower values for root tips, branching points, and total root length compared to both Paragon and Senatore Cappelli (all $p < 0.001$). Senatore Cappelli and Watkins238 presented significantly smaller average and maximum root diameter compared to Paragon ($p < 0.001$ and $p < 0.01$, respectively). Branching frequency was significantly lower in both Senatore Cappelli and Watkins238 compared to Paragon (both $p < 0.001$). Finally, the root length within diameter ranges 1 and 2 was significantly lower in Senatore Cappelli and Watkins238 compared to Paragon ($p < 0.01$ and $p < 0.001$, respectively).

### 3.2. Minkowski functionals and percolation properties

#### 3.2.1. Cylinder scale, total imaged porosity

No statistically significant differences were observed among the cultivars or between the bare and rhizospheric soil for the geometric and topological characteristics of the Minkowski functionals (Fig. 4). The analysis of the critical diameter at the cylinder scale did not reveal any significant differences between the samples, with a mean value of 0.06 mm.

From the analysis of total imaged porosity, the only parameter non-normally distributed was the connection probability and the values, for both rhizosphere and bare soil samples were comparable and showed no significant differences. The percolation threshold is the minimum porosity required within the analyzed volume to form at least one "percolating" cluster, i.e., a cluster that spans from one end to the other of a 3D image in a finite system, such as our tomography-scanned volume. This parameter does not depend solely on the amount of porosity but also on morphological properties of the pore network, such as anisotropy (Jarvis et al., 2017) and pore size distribution (Huang et al., 2021). Consequently, higher connectivity is often associated with a lower percolation threshold. The percolation threshold revealed notable differences between rhizospheric and bare soil samples (Fig. 5), being significantly higher in bare soil ($p < 0.01$) than in rhizospheric soil. The observation of similar total connection probabilities between rhizospheric and control soils, along with significantly higher percolation threshold values for bare soil, suggests that bare soil contains clusters large enough to support connectivity comparable to that of root-explored soils. However, these clusters are less uniformly distributed within the volume, resulting in lower levels of percolation compared to rhizospheric soil.

This highlights the importance of using a broad set of parameters to describe the morphology of the pore phase from multiple perspectives. Since a high percolation threshold indicates highly disconnected porosity or non-conducting regions (Daigle et al., 2019; Soto-Gómez et al., 2020), this finding evidences the beneficial effect of wheat roots on soil structure. Root activity promotes a more connected pore network, reducing the percolation threshold and enhancing total connectivity. Our results are consistent with Lucas et al. (2019a), who

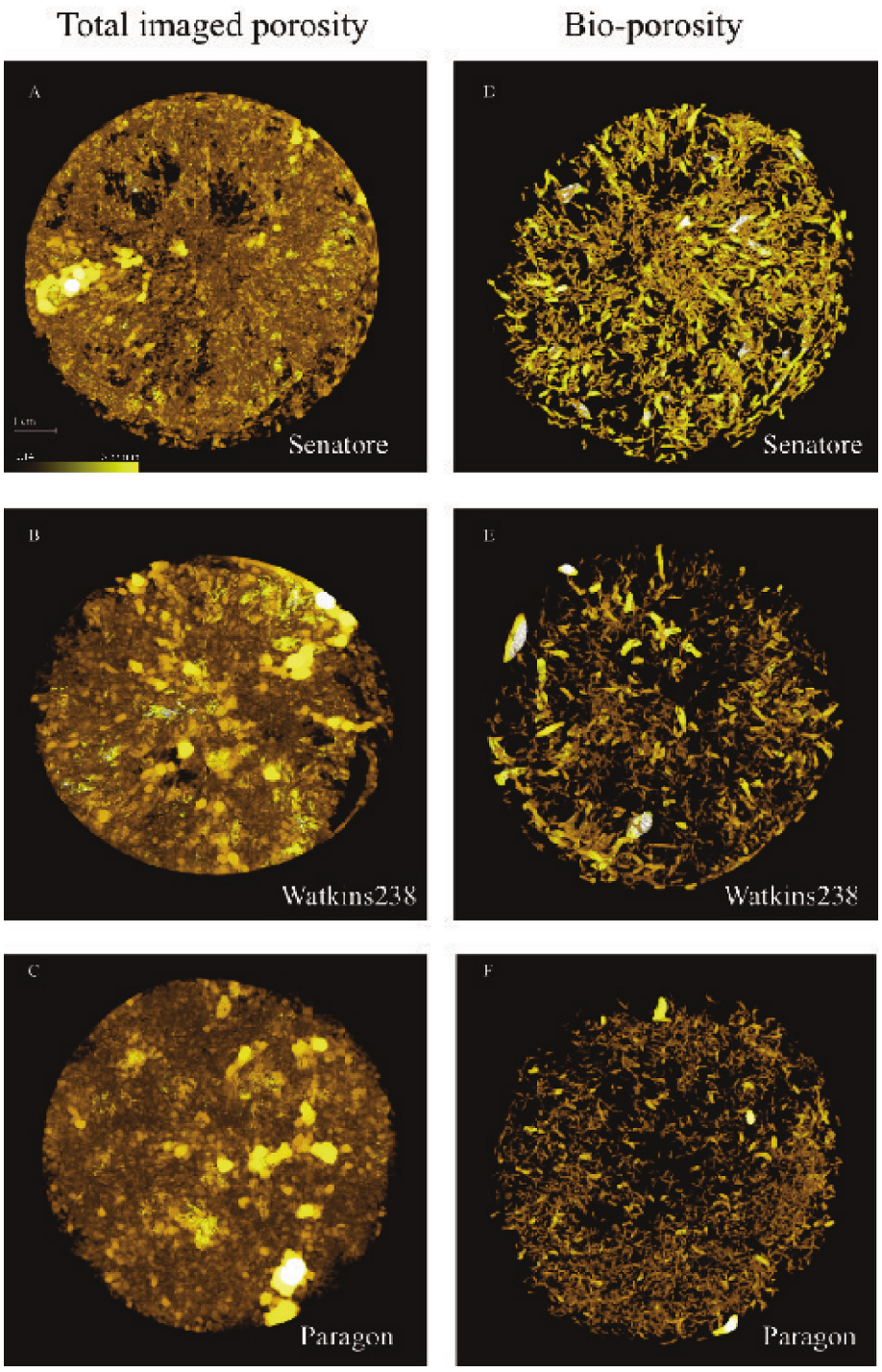


**Fig. 6.** Tomographic images of total imaged porosity and bioporosity for the three cultivars for the one representative cylinder sample. The color gradient is a representation of the pore diameter.

emphasized the critical role of connected pores formation in plant growth that facilitates access to deeper soil layers and mitigates the impact of soil compaction.

### 3.2.2. *Cylinder scale, bioporosity*

Xiong et al. (2022), stated the importance of biopores smaller than 2 mm, which is the case of the ones observed at both scales in this study, since they consistently promote plant growth by enhancing root-soil interactions, nutrient uptake, and water absorption. The bioporosity network is presented in Fig. 6, while Fig. 7 illustrates the morphological functions (MFs) for the biopore networks at both the cylinder and aggregate scales. No significant differences were observed between rhizospheric and bare soils in terms of total biopore volume fraction, mean curvature, or surface area.

### 3.2.3. *Cylinder scale, pore size distributions*

The computed frequency distribution of the pore diameters (Fig. 8) extracted from cylinder samples span a pore diameter range from 0.15 to 3 mm and it was fitted with an Inverse Gamma distribution. Each distribution was compared among the samples using the Kolmogorov-Smirnov test and the results revealed significant differences for the following pairs: Senatore-Cappelli and Paragon ($p < 0.01$), Senatore-

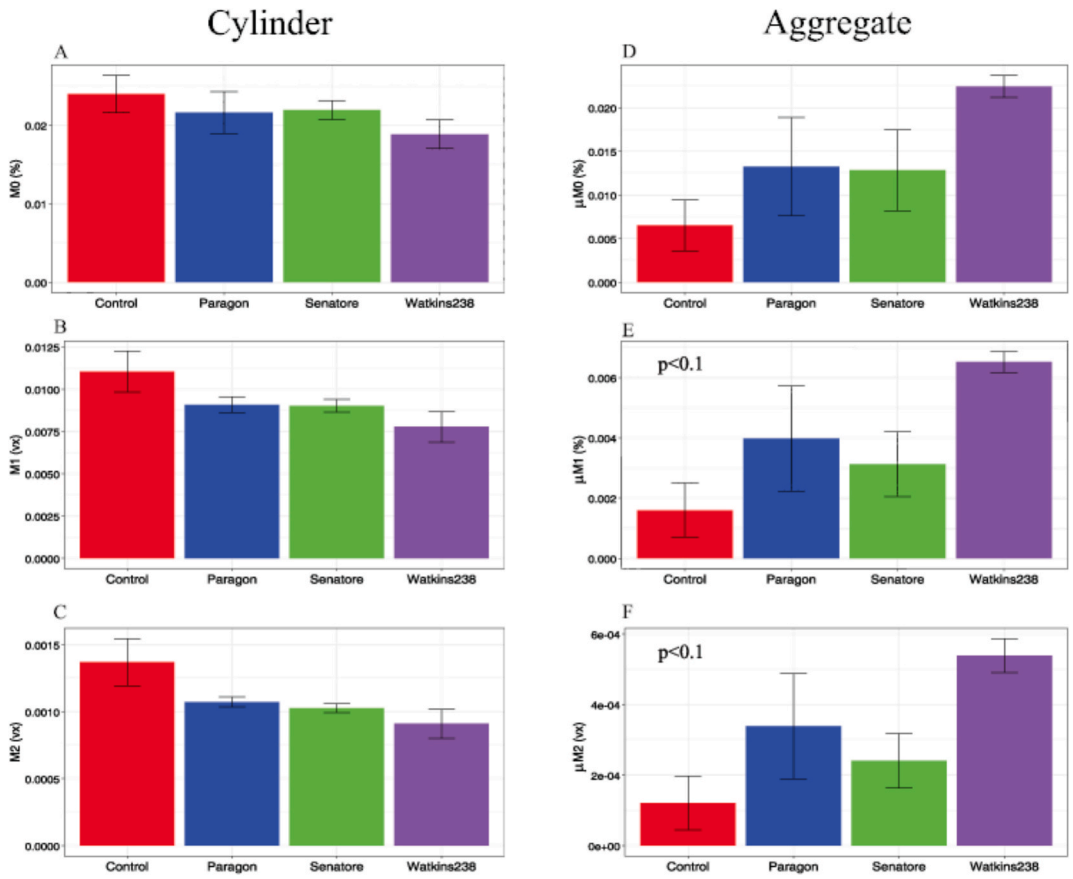


**Fig. 7.** Values of M0 (biopore volume), M1 (surface area), M2 (mean curvature) for the cylinder and the aggregate, for the control and three cultivars. The values are computed for the imaged bioporosity.

Cappelli and Watkins238 ($p < 0.01$), Watkins238 and bare soil ($p < 0.01$), and Senatore-Cappelli and bare soil ($p < 0.1$).

To better visualize these differences, all soils were characterized by total imaged biopore diameters below 3 mm (Fig. 9) in a cumulative curve, with the most abundant diameters ranging between 0.45 and 0.8 mm.

We found a significant difference in biopore size distributions between Senatore-Cappelli and Watkins238 ($p < 0.05$), with the latter one having smaller diameters. Bioporosity volumes between control and rizospheric soil within this diameter range are comparable (Fig. 7) indicating that the biopores produced by spontaneous vegetation from the previous year were still persistent, and the diameters in the bare soil samples were smaller compared to the rhizospheric soil ($p < 0.01$ both for Senatore-Cappelli and Paragon respect control) (Fig. 9), which confirms the findings of Whalley et al. (2005). This is likely due to the creation of larger pores by wheat root growth.

### 3.2.4. *Aggregate scale, total imaged porosity*

For the total imaged porosity at the aggregate scale, no statistically significant differences were observed among the rhizospheric and the bare soil, although the porosity values within the aggregate suggested that the presence of roots might result in a larger pore volume fraction ($p = 0.11$) and greater imaged pore connectivity, as indicated by lower Euler numbers (Fig. 4) Similarly to what we observed for the cylinder samples, the non-normally distributed percolation theory parameter (Fig. 5) showed significant differences between rhizospheric samples and bare soil, the percolation threshold was higher in the control samples than in the rhizospheric values ($p < 0.01$). These results indicate that, although rhizospheric soil is known to be more compacted than bulk soil (Dexter, 1988, Whalley et al., 2005; Daly et al., 2015; Lucas et al., 2019a) it also exhibits a more connected structure (Helliwell et al., 2019), with roots promoting enhanced structural connectivity across the two scales assessed.

### 3.2.5. *Aggregate scale, bioporosity*

Bioporosity inside the aggregate is likely determined by the growth of fine roots (Hendriks et al., 2022) (Fig. 10). In the aggregate samples, no significant differences were found for the total bioporosity fraction parameter. However, the results suggest a lower bioporosity fraction in the bare soil samples. Since this pattern was not observed at the cylinder scale, we speculate that bioporosity associated with fine root growth may be less persistent than that associated with larger roots. Interestingly, the cultivar Watkins238 showed higher values for surface area ($p < 0.1$) and mean curvature ($p < 0.1$) of the aggregates compared to bare soil samples. These two functionals likely enhance the development of the microbiome and increase the surface area available that roots encounter for exchanges of nutrients, gases and water fluxes (San Josè Martinez et al., 2015).

### 3.2.6. *Aggregate scale, pore size distribution*

For pore diameters ranging between 0.03 mm and 1.5 mm, the Inverse Gamma model fitting was not performed on the control samples (Fig. 9), since as indicated in Figs. 4 and 7 there was an order-of-magnitude difference in porosity between the bare and the rhizospheric soil. Consequently, illustrating a distribution function across such different volumes would not provide a representative comparison. The pairwise comparisons among the rhizospheric samples showed significant differences for Watkins238 vs. Senatore-Cappelli ($p < 0.01$) and Watkins238 vs. Paragon ($p < 0.01$). Analysis of the biopores at this resolution resulted in significant differences for Senatore-Cappelli vs. Watkins238 ($p < 0.01$) and Senatore-Cappelli vs. Paragon ($p < 0.01$). Similarly, to the bioporosity investigated in the larger diameter range,

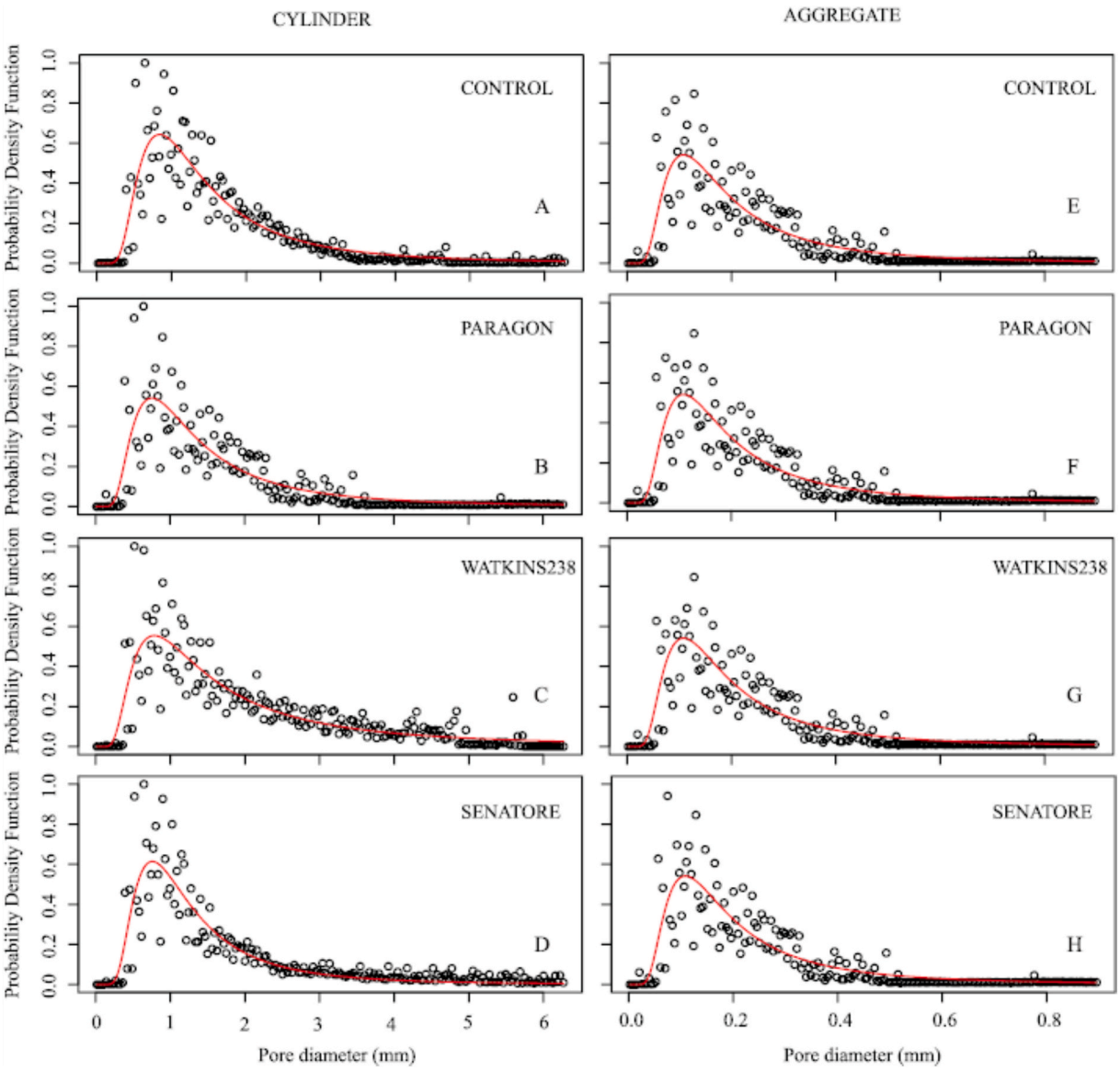


**Fig. 8.** Probability density function (PDF) for the cylinder and aggregate samples, for the control and three cultivar samples. The red line was obtained by fitting the inverse gamma function to the experimental data (dots).

Senatore-Cappelli consistently exhibited slower increase in the curves, with 90 % of bioporosity below 1 mm compared to 97 % for both Watkins238 and Paragon. The Paragon and Watkins238 cultivars, which have thicker roots, may cause greater compaction of the rhizospheric soil during exploration in this size range, which may ultimately lead to enhanced soil microporosity as root decay. During the decomposition process, the substantial loss of water from roots and root hairs causes a reduction in their diameter, creating voids previously occupied by the root structures, which are subsequently filled with air (Lucas, 2022). These voids, or biopores, improve soil structure by enhancing aeration, water infiltration, and retention. Furthermore, the decomposition of roots enriches the biopore walls with nutrients and promotes microbial activity, creating hotspots for nutrient cycling and contributing to soil health and fertility (Wendel et al., 2022), and potentially enhancing water retention and structural stability at this scale. This behavior, and our results indicating that soil underwent compaction for pores in the range between 0.1 and 0.5 mm, are consistent with previous research reporting that roots decrease porosity in rhizosphere plots, especially for macropores (>0.25 mm) (Lucas et al., 2019a). The authors indicated that these effects depend on the initial bulk density, but that bulk density alone is not sufficient to explain this complex behavior. This was also discussed by Dexter (2004), who reported that compaction around roots also depends on other soil physical properties such as the organic matter content and water retention capacity. The authors maintained that the ability of the roots to grow into an already connected soil affects the eventual impact on the pore size distribution. Therefore, the connectivity parameters measured in the overall imaged pore system are not only influenced by plant roots but also shape their growth, creating a dynamic relationship of mutual influence. These results may explain the scale dependent effect on the imaged pore size distribution of the three wheat cultivars that was found between the pore size ranges of 0.05 to 0.5 mm (aggregate) and 0.5 to 2 mm (cylinder), and demonstrates that the influence of the root morphology on the physical properties of a particular soil varies depending on the pore size range analyzed.

### 3.3. *Root traits impact on total imaged porosity*

The ANOVA results show that the root traits of the cultivars mainly affect the percolation threshold for both cylinder and aggregate scale, with bare soil displaying significantly higher values than Paragon,

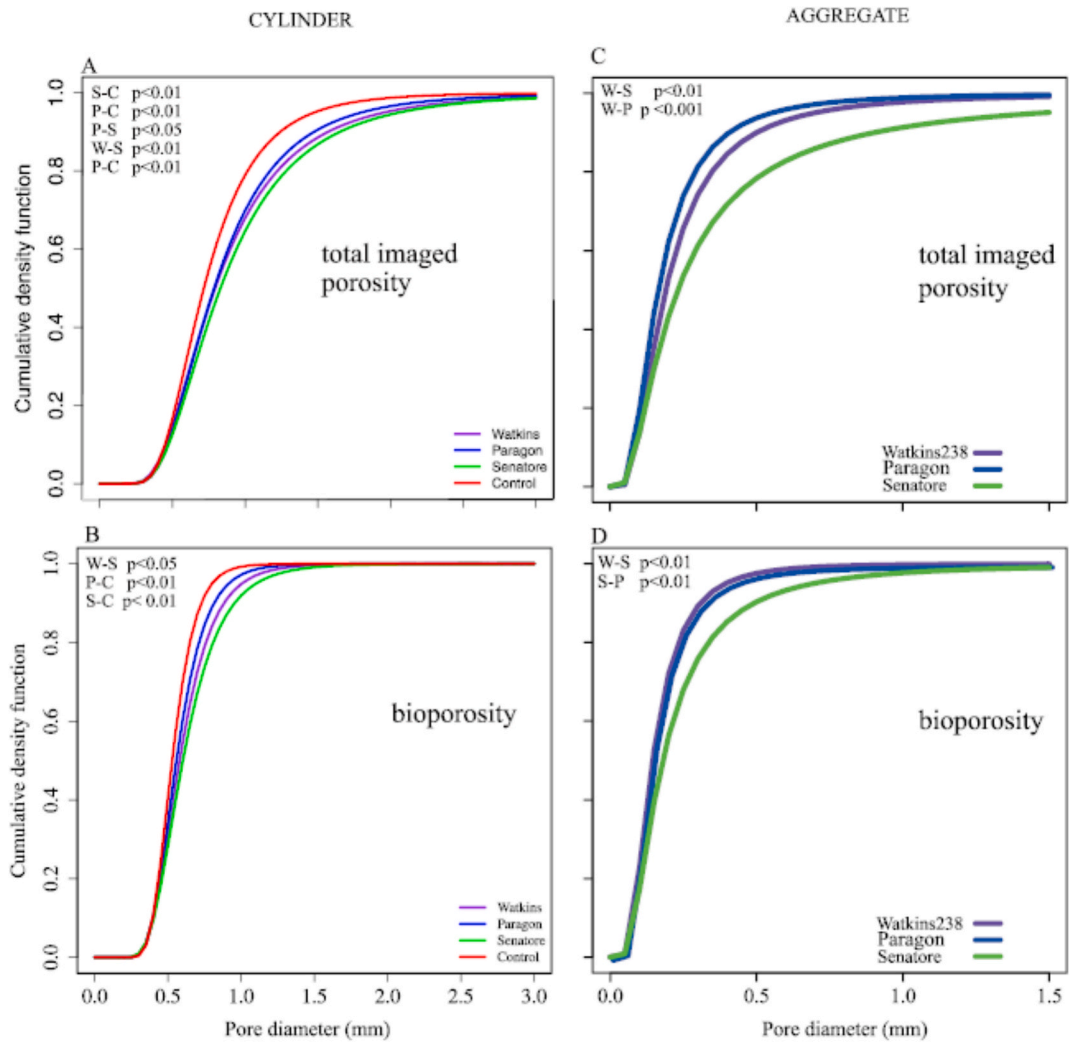


**Fig. 9.** Modeled cumulative distribution functions for total imaged and bio-porosity for the cylinder and aggregate samples. Both curves are represented on a scale that allows visualization of their growth up to approximately 95%, for a better comparison of their differences.

Senatore Cappelli, and Watkins238 ($p < 0.01$). These results suggest that the cultivars Paragon, Senatore Cappelli, and Watkins238 might modify specific soil characteristics. Tukey's post hoc tests confirmed these differences, suggesting a negative effect of bare soil on soil permeability. These findings are relevant to advancing our capability to introduce root traits with potential to influence the soil structure. Particular root traits showed specific correlation on soil properties (Fig. 11), showing how specific root trait could be correlated with specific soil physical property. Crown network area was positively associated with M0 ($p < 0.05$), M1 ($p = 0.05$), GAMMA ($p < 0.05$), and μPT ($p < 0.001$), while negatively affecting M2 ($p < 0.05$). Those correlations suggests decreased bulk density in the rhizospheric zone, this being consistent with previous research (Aravena et al., 2011; Lucas et al., 2019a; Helliwell et al. 2019, Phalempin et al., 2021) that reported compaction around the growing roots.

Shallow angle frequency was positively associated with GAMMA ($p < 0.05$), whereas steep angle frequency was negatively correlated with the same parameter ($p < 0.05$).

Branching frequency showed contrasting effects depending on the soil variable. It was positively associated with M0 ($p < 0.01$), M1 ($p < 0.001$), and GAMMA ($p < 0.01$), while showing a significant negative correlation with M3 ($p < 0.01$). A weaker negative association was also found with μGAMMA ($p = 0.05$).

Root diameter presented a positive relationship with M0 ($p < 0.05$), M1 ($p < 0.001$), and GAMMA ($p = 0.05$), while being negatively correlated with M3 ($p < 0.01$). Maximum root diameter had a positive effect on M0 ($p < 0.05$), M1 ($p = 0.05$), GAMMA ($p < 0.05$), and μM3 ($p < 0.05$), while showing a negative correlation with M2 ($p < 0.05$). Those correlations suggest that thicker roots could decrease bulk density, confirming previous studies results (Aravena et al., 2011; Lucas et al., 2019a; Helliwell et al. 2019, Phalempin et al., 2021). Our results confirmed that root diameter might affect multiple soil properties, as previously suggested by Lu et al. (2020).

### 3.4. *Root traits impact on soil bioporosity*

The effect of the different root traits on the bioporosity morphology was assessed by combining the root features of the three genotypes and tested for correlation with each bioporosity parameter. Fig. 12 depicts the root traits that presented a statistically significant effect on bioporosity.

At the aggregate scale, branching frequency and root length were positively associated with μM0 ($p < 0.05$). At the cylinder scale, root diameter and branching frequency were positively associated with M0 ($p < 0.05$). FRMP exhibited a strong negative correlation with M0, M1, and M2 ($p < 0.01$). Interestingly, tap root length and root length showed weak positive correlations with M2 and M3 ($p = 0.05$). Shallow angle frequency was negatively associated with M1, M2. In contrast, steep

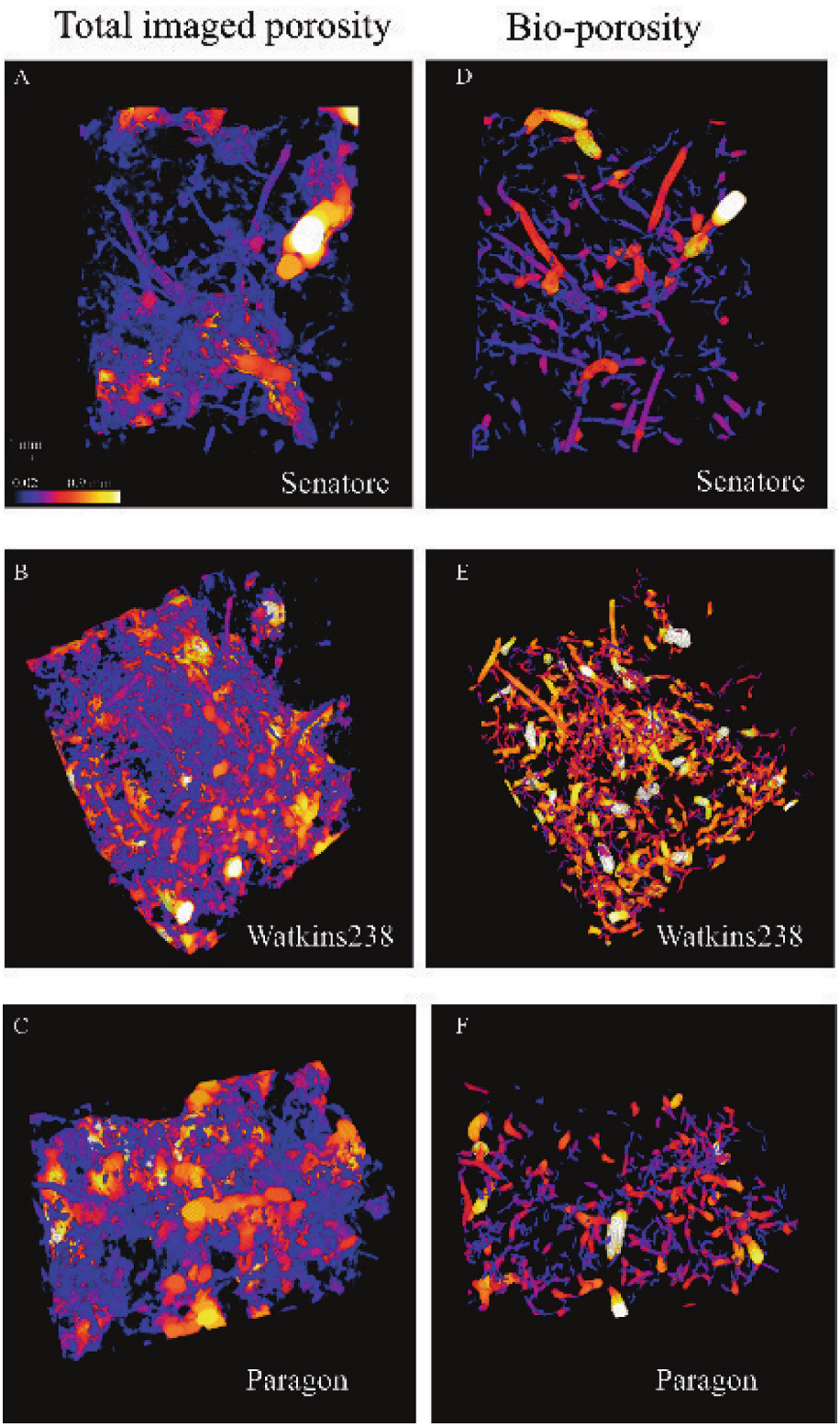


**Fig. 10.** Tomographic images of total imaged porosity and bioporosity of the three cultivars for the one representative aggregate sample. The color shades represent the pore diameter.

angle frequency was positively correlated with M1 and M2.

## 4. Conclusion

This study provides further insight into the potential influence of wheat root traits on soil physical properties, particularly on the pore network structure. By combining non-destructive X-ray tomography with 2D root phenotyping, we explored how different genotypes may contribute to modifying soil structure under controlled conditions. While no significant differences were detected in total porosity, our findings suggest that root development can enhance pore connectivity and reduce the percolation threshold, potentially improving water and

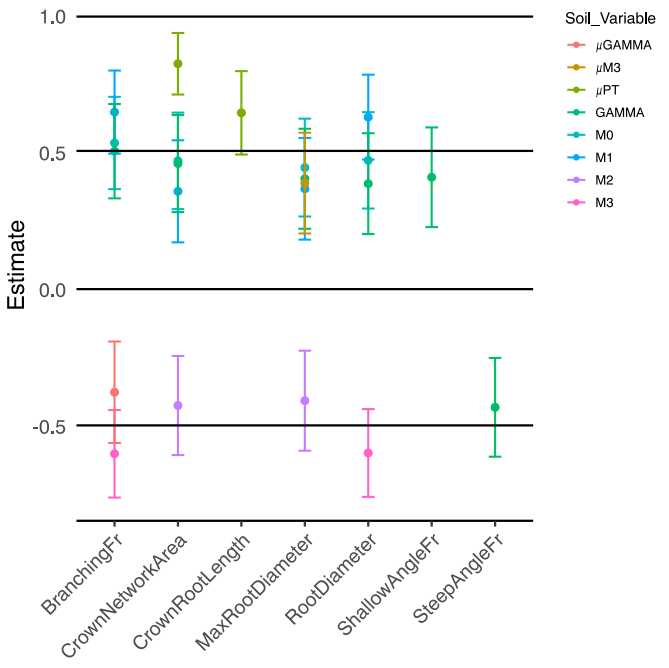


**Fig. 11.** Effect of each root trait on the statistically significant soil morphological parameters obtained by using a mixed linear model, on total imaged porosity. When a parameter does not show it means it was not statistically significant. Symbols for the root are Avg = Average Root Diameter, Frmp = Fragmented Root Morphological Pattern, NuRT = Number of Root Tips, Per = Perimeter, ShaF/SteepF = Shallow and Steep Angle Frequency, TotaL = Total Root Length, Vol = Root Volume.

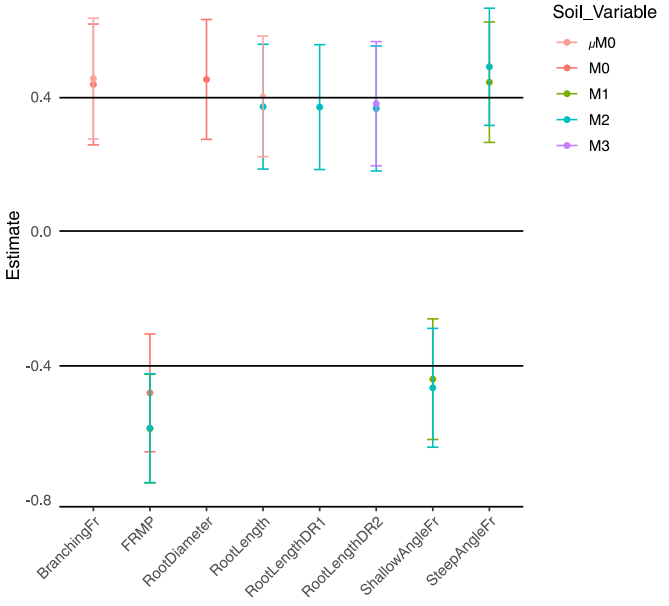


**Fig. 12.** Effect of each root trait on the statistically significant soil morphological parameters obtained by using a mixed linear model, on bioporosity. When a parameter does not show it means it was not statistically significant. Symbols for the root are Avg = Average Root Diameter, Frmp = Fragmented Root Morphological Pattern, NuRT = Number of Root Tips, Per = Perimeter, ShaF/SteepF = Shallow and Steep Angle Frequency, TotaL = Total Root Length, Vol = Root Volume.

air transport within the soil. Differences in bioporosity distribution across genotypes and scales indicate that root system morphology, including traits such as diameter, branching frequency, and root length, may play a role in shaping the rhizospheric soil. However, the observed effects appear to be scale-dependent and may vary with root persistence, compaction, and post-harvest decomposition processes. Further research is needed to validate these patterns under field conditions and assess the long-term implications of root traits on soil structure and functionality.

## CRediT authorship contribution statement

**Bartolo Giuseppe Dimattia:** Conceptualization, Data curation, Formal analysis, Investigation, Methodology, Software, Writing – original draft, Writing – review & editing. **Angela Righi:** Data curation, Formal analysis, Investigation, Methodology, Software, Visualization, Writing – original draft, Writing – review & editing. **Matteo Bettuzzi:** Data curation, Investigation, Methodology, Writing – original draft. **John Koestel:** Investigation, Methodology, Software, Validation, Visualization, Writing – original draft, Writing – review & editing. **Maria Pia Morigi:** Investigation, Methodology, Resources. **Rosa Brancaccio:** Investigation, Methodology, Software. **Silvio Salvi:** Conceptualization, Funding acquisition, Project administration, Resources, Supervision, Writing – original draft, Writing – review & editing. **Maria C. Hernandez-Soriano:** Conceptualization, Funding acquisition, Project administration, Resources, Supervision, Writing – original draft, Writing – review & editing. **Marco Bittelli:** Conceptualization, Data curation, Formal analysis, Funding acquisition, Methodology, Project administration, Supervision, Validation, Writing – original draft, Writing – review & editing.

## Declaration of competing interest

The authors declare that they have no known competing financial interests or personal relationships that could have appeared to influence the work reported in this paper.

## Acknowledgements

The research was partially funded by the project WISH-ROOTS- "Tuning the wheat root microbiome to improve soil health and optimize rhizosphere nitrogen cycling and availability" is supported by the European Join Programme Soil ERA- NET (HORIZON 2020) research and innovation programme. MCHS gratefully acknowledges funding support from the Biotechnology and Biological Sciences Research Council (BBSRC), project BB/X003000/1. Funding was also provided by the Department of Agricultural and Food Sciences, University of Bologna, through its Ph.D programme. We thank Roberto Tuberosa for useful discussion and for participation in the development and implementation of the funded project. We are also grateful to Marco Maccaferri for providing the seeds of the cultivar Senatore-Cappelli and for useful discussions, to the John Innes Centre Germplasm Resources Unit for providing the seeds of the Paragon and Watkins238 cultivars, and to Simon Griffiths and Luzie Wingen for advice on the relevance of these cultivars.

Additional support to Bartolo Giuseppe Dimattia was provided by the Collegio Superiore and the Institute of Advanced Studies of the University of Bologna, whose contribution is gratefully acknowledged.

### *Author contributions statement*

B.G.D. contributed to the writing of the funded project, conceived the experiment, followed all the agronomic practices and management practices, collected samples and data, analyzed the data and contributed to the writing of the paper, A.R. collected the samples, performed X-ray measurements, image and statistical analysis and contributed to the writing of the paper , M.B, M.P.M. and R.B are responsible for the X-ray center and performed the X-ray imaging, J.K. is the developer of the SoilJ plugin used for image analysis, contributed to image analysis and

manuscript review and writing, S.S. is the responsible for the Bologna group of the project and contributed to the field experiment, M.C.H.S is the coordinator of the project and contributed to manuscript review, and M.B contributed to the writing of the funded project, contributed to the project coordination, to the experimental setup design, to data analysis and writing of the paper.

## Appendix A. Supplementary data

Supplementary data to this article can be found online at https://doi.org/10.1016/j.geoderma.2025.117349.

## Data availability

Data will be made available on request.

## References


Angers, D.A., Caron, J., 1998. Plant-induced changes in soil structure: processes and feedbacks. Biogeochemistry 42, 55–72. https://doi.org/10.1023/A:1005944025343.

Aravena, J.E., Berli, M., Ghezzehei, T.A., Tyler, S.W., 2011. Effects of root-induced compaction on rhizosphere hydraulic properties—X-ray microtomography imaging and numerical simulations. Environ. Sci. Tech. 45, 425–431. https://doi.org/10.1021/es102566j.

Armstrong, R.T., McClure, J.E., Robins, V., Liu, Z., Arns, C.H., Schlüter, S., Berg, S., 2018. Porous media characterization using Minkowski functionals: theories, applications and future directions. Transp. Porous Media 123, 619–649. https://doi.org/10.1007/s11242-018-1201-4.

Balashov, E., Bazzoffi, P., 2003. Aggregate water stability of sandy and clayey loam soils differently compacted with and without wheat plants. Int. Agrophys. 17, 151–155.

Bardgett, R.D., Mommer, L., De Vries, F.T., 2014. Going underground: root traits as drivers of ecosystem processes. Trends Ecol. Evol. 29, 692–699. https://doi.org/10.1016/j.tree.2014.10.006.

Bittelli, M., Campbell, G.S., Tomei, F., 2015. Soil Physics with Python: Transport in the Soil-Plant-Atmosphere Continuum. Oxford University Press, Oxford, UK.

Bodner, G., Leitner, D., Kaul, H.P., 2014. Coarse and fine root plants affect pore size distributions differently. Plant Soil 380, 133–151. https://doi.org/10.1007/s11104-014-2079-8.

Brancaccio, R., Bettuzzi, M., Casali, F., Morigi, M.P., Levi, G., Gallo, A., Marchetti, G., Schneberk, D., 2011. Real-time reconstruction for 3D CT applied to large objects of cultural heritage. IEEE Trans. Nucl. Sci. 58, 1864–1871. https://doi.org/10.1109/TNS.2011.2158850.

Brussaard, L., 2012. Ecosystem services provided by the soil biota. In: Wall, D.H. (Ed.), Soil Ecology and Ecosystem Services. Oxford University Press, Oxford, UK, pp. 45–58. https://doi.org/10.1093/acprof:oso/9780199575923.003.0005.

Buades, A., Coll, B., Morel, J.M., 2011. Non-local means denoising. Image Process Online 1, 208–212. https://doi.org/10.5201/ipol.2011.bcm_nlm.

Bucksch, A., Burridge, J., York, L.M., Das, A., Nord, E.A., Weitz, J.S., Lynch, J.P., 2014. Image-based high-throughput field phenotyping of crop roots. Plant Physiol. 166, 470–486. https://doi.org/10.1104/pp.114.243519.

Burr-Hersey, J.E., Ritz, K., Bengough, G.A., Mooney, S.J., 2020. Reorganisation of rhizosphere soil pore structure by wild plant species in compacted soils. J. Exp. Bot. 71, 6107–6115. https://doi.org/10.1093/jxb/eraa323.

Carminati, A., Moradi, A., Vetterlein, D., 2010. Dynamics of soil water content in the rhizosphere. Plant Soil 332, 163–176. https://doi.org/10.1007/s11104-010-0283-8.

Cheng, S., Feng, C., Wingen, L.U., et al., 2024. Harnessing landrace diversity empowers wheat breeding. Nature 632, 823–831. https://doi.org/10.1038/s41586-024-07682-9.

Childs, E.C., Collis-George, N., 1948. Soil geometry and soil-water equilibria. Discuss. Faraday Soc. 3, 78–85. https://doi.org/10.1039/DF9480300078.

Daigle, H., Reece, J.S., Flemings, P.B., 2019. Evolution of the percolation threshold in muds and mudrocks during burial. Geophys. Res. Lett. 46, 5966–5973. https://doi.org/10.1029/2019GL083723.

Dal Ferro, N., Sartori, L., Simonetti, G., Berti, A., Morari, F., 2014. Soil macro- and microstructure as affected by different tillage systems and their effects on maize root growth. Soil Tillage Res. 140, 55–65. https://doi.org/10.1016/j.still.2014.02.003.

Daly, K.R., Mooney, S.J., Bennett, M., Crout, N.M.J., Roose, T., Tracy, S.R., 2015. Assessing the influence of the rhizosphere on soil hydraulic properties using X-ray computed tomography and numerical modelling. J. Exp. Bot. 66, 2305–2314. https://doi.org/10.1093/jxb/eru509.

De La Fuente Cantó, C., Simonin, M., King, E., Moulin, L., Bennett, M.J., Castrillo, G., Laplaze, L., 2020. An extended root phenotype: the rhizosphere, its formation and impacts on plant fitness. Plant J. 103, 951–964. https://doi.org/10.1111/tpj.14781.

Dexter, A.R., 1988. Advances in characterization of soil structure. Soil Tillage Res. 11, 199–238. https://doi.org/10.1016/0167-1987(88)90002-5.

Dinno, A. 2024. Conover.test: Conover-Iman Test of Multiple Comparisons Using Rank Sums. R package version 1.1.6.

Giuliani, L.M., Hallett, P.D., Loades, K.W., 2024. Effects of soil structure complexity to root growth of plants with contrasting root architecture. Soil Tillage Res. 238, 106023. https://doi.org/10.1016/j.still.2024.106023.

Helliwell, J.R., Sturrock, C.J., Miller, A.J., Whalley, W.R., Mooney, S.J., 2019. The role of plant species and soil condition in the structural development of the rhizosphere. Plant Cell Environ. 42, 1974–1986. https://doi.org/10.1111/pce.13529.

Hendriks, P.M., Ryan, P., Hands, P., Rolland, V., Gurusinghe, S., Weston, L., Rebetzke, G., Delhaize, E., 2022. Selection for early shoot vigour in wheat increases root hair length but reduces epidermal cell size of roots and leaves. J. Exp. Bot. 73, 1672–1684. https://doi.org/10.1093/jxb/erac048.

Horn, R., Taubner, H., Wuttke, M., Baumgartl, T., 1994. Soil physical properties related to soil structure. Soil Tillage Res. 30, 187–216. https://doi.org/10.1016/0167-1987(94)90005-1.

Huang, L.K., Wang, M.J.J., 1995. Image thresholding by minimizing the measures of fuzziness. Pattern Recogn. 28, 41–51. https://doi.org/10.1016/0031-3203(94)E0043-K.

Huang, X., Yang, D., Kang, Z., 2021. Impact of pore distribution characteristics on percolation threshold based on site percolation theory. Physica A 570, 125800. https://doi.org/10.1016/j.physa.2021.125800.

Hunt, A.G., Ewing, R.P., Horton, R., 2013. What's wrong with soil physics? Soil Sci. Soc. Am. J., 77, 1877–1887. https://doi.org/10.2136/sssaj2013.01.0020.

Jarvis, N., Larsbo, M., Koestel, J., 2017. Connectivity and percolation of structural pore networks in a cultivated silt loam soil quantified by X-ray tomography. Geoderma 287, 71–79. https://doi.org/10.1016/j.geoderma.2016.06.026.

Kahle, D., Stamey, J., 2017. invgamma: The Inverse Gamma Distribution. R Package Version 1, 1.

Kan, X., Zheng, W., Cheng, J., Zhang, L., Li, J., Liu, B., Zhang, X., 2023. Investigating soil pore network connectivity in varied vegetation types using X-ray tomography. Water 15, 3823. https://doi.org/10.3390/w15213823.

Kapur, J.N., Sahoo, P.K., Wong, A.K.C., 1985. A new method for gray-level picture thresholding using the entropy of the histogram. Comput. Vision Graph. Image Process. 29, 273–285. https://doi.org/10.1016/0734-189X(85)90125-2.

Koestel, J., 2018. SoilJ: An ImageJ plugin for the semiautomatic processing of three-dimensional X-ray images of soils. Vadose Zone J. 17, 1–7. https://doi.org/10.2136/vzj2017.03.0062.

Koestel, J., Dathe, A., Skaggs, T.H., Klakegg, O., Ahmad, M.A., Babko, M., Giménez, D., Farkas, C., Nemes, A., Jarvis, N., 2018. Estimating the permeability of naturally structured soil from percolation theory and pore space characteristics imaged by X-ray computed tomography. Water Resour. Res. 54, 2344–2360. https://doi.org/10.1029/2018WR023609.

Koestel, J., Larsbo, M., Jarvis, N., 2020. Scale and REV analyses for porosity and pore connectivity measures in undisturbed soil. Geoderma 366, 114206. https://doi.org/10.1016/j.geoderma.2020.114206.

Kravchenko, A.N., Guber, A.K., 2017. Soil pores and their contributions to soil carbon processes. Geoderma 287, 31–39. https://doi.org/10.1016/j.geoderma.2016.06.027.

Kuka, K., Illerhaus, B., Fox, C.A., Joschko, M., 2013. X-ray computed microtomography for the study of the soil–root relationship in grassland soils. Vadose Zone J. 12, 1–10. https://doi.org/10.2136/vzj2013.01.0014.

Lal, R., 2009. Soil and world food security. Soil Tillage Res. 102, 1–4. https://doi.org/10.1016/j.still.2008.08.001.

Lal, R., 2015. Restoring soil quality to mitigate soil degradation. Sustainability 7, 5875–5895. https://doi.org/10.3390/su7055875.

Le Marié, C.A., York, L.M., Strigens, A., Malosetti, M., Camp, K.H., Giuliani, S., Lynch, J. P., Hund, A., 2019. Shovelomics root traits assessed on the EURoot maize panel are highly heritable across environments but show low genotype-by-nitrogen interaction. Euphytica 215, 173. https://doi.org/10.1007/s10681-019-2472-8.

Leue, M., Uteau-Puschmann, D., Peth, S., Nellesen, J., Kodešová, R., Gerke, H.H., 2019. Separation of soil macropore types in three-dimensional X-ray computed tomography images based on pore geometry characteristics. Vadose Zone J. 18, 180170. https://doi.org/10.2136/vzj2018.09.0170.

Liu, J., Regenauer-Lieb, K., 2011. Application of percolation theory to microtomography of structured media: percolation threshold, critical exponents, and upscaling. Phys. Rev. E 83, 016106. https://doi.org/10.1103/PhysRevE.83.016106.

Liu, S., Barrow, C.S., Hanlon, M., Lynch, J.P., Bucksch, A., 2021. DIRT/3D: 3D root phenotyping for field-grown maize (Zea mays). Plant Physiol. 187 (2), 739–757. https://doi.org/10.1093/plphys/kiab311.

Logsdon, S.D., 2013. Root effects on soil properties and processes: synthesis and future research needs. Adv. Agric. Syst. Model., 4, 173–196. https://doi.org/10.2134/advagricsystmodel4.c8.

Lu, J., Zhang, Q., Werner, A.D., Li, Y., Jiang, S., Tan, Z., 2020. Root-induced changes of soil hydraulic properties – a review. J. Hydrol. 589, 125203. https://doi.org/10.1016/j.jhydrol.2020.125203.

Lucas, M., Schlüter, S., Vogel, H.J., Vetterlein, D., 2019a. Roots compact the surrounding soil depending on the structures they encounter. Sci. Rep. 9, 16236. https://doi.org/10.1038/s41598-019-52665-w.

Lucas, M., Schlüter, S., Vogel, H.J., Vetterlein, D., 2019b. Soil structure formation along an agricultural chronosequence. Geoderma 350, 87–97. https://doi.org/10.1016/j.geoderma.2019.04.041.

Lucas, M., 2022. Perspectives from the Fritz-Scheffer Awardee 2020—the mutual interactions between roots and soil structure and how these affect rhizosphere processes. J. Plant Nutr. Soil Sci. 185, 8–18.

Lynch, J.P., 2022. Harnessing root architecture to address global challenges. Plant J. 109, 415–431. https://doi.org/10.1111/tpj.15560.

Maccaferri, M., El-Feki, W., Nazemi, G., Salvi, S., Canè, M.A., Colalongo, M.C., Stefanelli, S., Tuberosa, R., 2016. Prioritizing quantitative trait loci for root system architecture in tetraploid wheat. J. Exp. Bot. 67, 1161–1178. https://doi.org/10.1093/jxb/erw039.

Marone, D., Russo, M.A., Mores, A., Ficco, D.B., Laidò, G., Mastrangelo, A.M., Borrelli, G. M., 2021. Importance of landraces in cereal breeding for stress tolerance. Plants 10, 1267. https://doi.org/10.3390/plants10071267.
Mawodza, T., Burca, G., Casson, S., Menon, M., 2020. Wheat root system architecture and soil moisture distribution in an aggregated soil using neutron computed tomography. Geoderma 359, 113988. https://doi.org/10.1016/j.geoderma.2019.113988.
Mazzucotelli, E., et al., 2020. The global durum wheat panel (GDP): an international platform to identify and exchange beneficial alleles. Front. Plant Sci. 11, 569905. https://doi.org/10.3389/fpls.2020.569905.
Meysman, F.J.R., Middelburg, J.J., Heip, C.H.R., 2006. Bioturbation: a fresh look at Darwin's last idea. Trends Ecol. Evol. 21, 688–695. https://doi.org/10.1016/j.tree.2006.08.002.
Montanarella, L., Panagos, P., 2021. The relevance of sustainable soil management within the European Green Deal. Land Use Policy 100, 104950. https://doi.org/10.1016/j.landusepol.2020.104950.
Mooney, S.J., Pridmore, T.P., Helliwell, J., Bennett, M.J., 2012. Developing X-ray computed tomography to non-invasively image 3-D root systems architecture in soil. Plant Soil 352, 1–22. https://doi.org/10.1007/s11104-011-1039-9.
Nitzbon, J., Gadylyaev, D., Schlüter, S., Köhne, J.M., Grosse, G., Boike, J., 2022. Brief communication: Unravelling the composition and microstructure of a permafrost core using X-ray computed tomography. Cryosphere 16, 3507–3517. https://doi.org/10.5194/tc-16-3507-2022.
Ober, E.S., et al., 2021. Wheat root systems as a breeding target for climate resilience. Theor. Appl. Genet. 134, 1645–1662. https://doi.org/10.1007/s00122-021-03819-w.
Otsu, N., 1979. A threshold selection method from gray-level histograms. IEEE Trans. Syst. Man Cybern. 9, 62–66. https://doi.org/10.1109/TSMC.1979.4310076.
Pagliai, M., Vignozzi, N., 2002. The soil pore system as an indicator of soil quality. Adv. Geoecol. 35, 69–80.
Phalempin, M., Lippold, E., Vetterlein, D., Schlüter, S., 2021. Soil texture and structure heterogeneity predominantly governs bulk density gradients around roots. Vadose Zone J. 20, 5. https://doi.org/10.1002/vzj2.20147.
Prewitt, J.M.S., Mendelsohn, M.L., 1966. The analysis of cell images. Ann. N.Y. Acad. Sci. 128, 1035–1053. https://doi.org/10.1111/j.1749-6632.1965.tb11715.x.
Prince, S., Anower, M.R., Motes, C.M., Hernandez, T.D., Liao, F., Putman, L., Mattson, R., Seethepalli, A., Shah, K., Komp, M., Mehta, P., York, L.M., Young, C., Monteros, M.J., 2022. Intraspecific variation for leaf physiological and root morphological adaptation to drought stress in Alfalfa (Medicago sativa L.). Front. Plant Sci. 13, 795011. https://doi.org/10.3389/fpls.2022.795011.
Rabot, E., Wiesmeier, M., Schlüter, S., Vogel, H.J., 2018. Soil structure as an indicator of soil functions: a review. Geoderma 314, 122–137. https://doi.org/10.1016/j.geoderma.2017.11.009.
Renard, P., Allard, D., 2013. Connectivity metrics for subsurface flow and transport. Adv. Water Resour. 51, 168–196. https://doi.org/10.1016/j.advwatres.2011.12.001.
Ridler, T.W., Calvard, S., 1978. Picture thresholding using an iterative selection method. IEEE Trans. Syst. Man Cybern. 8, 630–632. https://doi.org/10.1109/TSMC.1978.4310039.
Ritchie, H., Roser, M., 2019. "Land Use" Published online at OurWorldinData.org. Retrieved from: https://ourworldindata.org/land-use [Online Resource].
RStudio Team, 2020. RStudio: Integrated Development Environment for R. RStudio. PBC, Boston, MA.
San Josè Martinez, F., Munoz Ortega, F.J., Caniego Monreal, F.J., Kravchenko, A.N., Wang, W., 2015. Soil aggregate geometry: Measurements and morphology. Geoderma 237, 36–48. https://doi.org/10.1016/j.geoderma.2014.08.003.
Schindelin, J., Arganda-Carreras, I., Frise, E., et al., 2012. Fiji: an open-source platform for biological-image analysis. Nat. Methods 9, 676–682. https://doi.org/10.1038/nmeth.2019.
Schlüter, S., Albrecht, L., Schwärzel, K., Kreiselmeier, J., 2020. Long-term effects of conventional tillage and no-tillage on saturated and near-saturated hydraulic conductivity – can their prediction be improved by pore metrics obtained with X-ray CT? Geoderma 361, 114082. https://doi.org/10.1016/j.geoderma.2019.114082.
Schlüter, S., Sheppard, A., Brown, K., Wildenschild, D., 2014. Image processing of multiphase images obtained via X-ray microtomography: a review. Water Resour. Res. 50, 3615–3639. https://doi.org/10.1002/2014WR015256.
Scholl, P., Leitner, D., Kammerer, G., Loiskandl, W., Kaul, H.P., Bodner, G., 2014. Root-induced changes of effective 1D hydraulic properties in a soil column. Plant Soil 381, 193–213. https://doi.org/10.1007/s11104-014-2119-4.
Seethepalli, A., Dhakal, K., Griffiths, M., Guo, H., Freschet, G.T., York, L.M., 2021. RhizoVision Explorer: open-source software for root image analysis and measurement standardization. AoB Plants 13, plab056. https://doi.org/10.1093/aobpla/plab056.
Shiferaw, B., Smale, M., Braun, H.J., Duveiller, E., Reynolds, M., Muricho, G., 2013. Crops that feed the world 10. Past successes and future challenges to the role played by wheat in global food security. Food Sec. 5, 291–317. https://doi.org/10.1007/s12571-013-0263-y.
Soto-Gómez, D., Juíz, L.V., Pérez-Rodríguez, P., López-Periago, J.E., Paradelo, M., Koestel, J., 2020. Percolation theory applied to soil tomography. Geoderma 357, 113959. https://doi.org/10.1016/j.geoderma.2019.113959.
Trachsel, S., Kaeppler, S.M., Brown, K.M., Lynch, J.P., 2011. Shovelomics: high throughput phenotyping of maize (Zea mays L.) root architecture in the field. Plant Soil 341, 75–87. https://doi.org/10.1007/s11104-010-0623-8.
Tracy, S.R., Black, C.R., Roberts, J.A., 2012. Quantifying the effect of soil compaction on three varieties of wheat (Triticum aestivum L.) using X-ray micro computed tomography (CT). Plant Soil 353, 195–208. https://doi.org/10.1007/s11104-011-1022-5.
Vogel, H.J., Weller, U., Schlüter, S., 2010. Quantification of soil structure based on Minkowski functions. Comput. Geosci. 36, 1236–1245. https://doi.org/10.1016/j.cageo.2010.03.007.
Wasson, A.P., Richards, R.A., Chatrath, R., Misra, S.C., Prasad, S.S., Rebetzke, G.J., Watt, M., 2012. Traits and selection strategies to improve root systems and water uptake in water-limited wheat crops. J. Exp. Bot. 63 (9), 3485–3498. https://doi.org/10.1093/jxb/ers111.
Weihs, B.J., Tang, Z., Tian, Z., Heuschele, D.J., Siddique, A., Terrill, T.H., Zhang, Z., York, L.M., Samac, D., Zhang, Z., Xu, Z., 2024. Phenotyping alfalfa (Medicago sativa L.) root structure architecture via integrating confident machine learning with ResNet-18. Plant Phenomics. https://doi.org/10.34133/plantphenomics.0251.
Wendel, A.S., Bauke, S.L., Amelung, W., Knief, C., 2022. Root-rhizosphere-soil interactions in biopores. Plant Soil 475, 253–277. https://doi.org/10.1007/s11104-022-05406-4.
Whalley, W.R., Riseley, B., Leeds-Harrison, P.B., Bird, N.R.A., Leech, P.K., Adderley, W. P., 2005. Structural differences between bulk and rhizosphere soil. Eur. J. Soil Sci. 56, 353–360. https://doi.org/10.1111/j.1365-2389.2004.00670.x.
Wingen, L.U., Orford, S., Goram, R., Leverington-Waite, M., Bilham, L., Patsiou, T.S., Ambrose, M., Dicks, J., Griffiths, S., 2014. Establishing the AE Watkins landrace cultivar collection as a resource for systematic gene discovery in bread wheat. Theor. Appl. Genet. 127, 1831–1842. https://doi.org/10.1007/s00122-014-2344-5.
Xiong, P., Zhang, Z., Peng, X., 2022. Root and root-derived biopore interactions in soils: a review. J. Plant Nutr. Soil Sci. 185 (5), 643–655. https://doi.org/10.1002/jpln.202200003.
Xu, Z., York, L.M., Seethepalli, A., Bucciarelli, B., Cheng, H., Samac, D.A., 2022. Objective phenotyping of root system architecture using image augmentation and machine learning in alfalfa (Medicago sativa L.). Plant Phenomics 9879610. https://doi.org/10.34133/2022/9879610.
Yen, J.C., Chang, F.J., Chang, S., 1995. A new criterion for automatic multilevel thresholding. IEEE Trans. Image Process. 4, 370–378. https://doi.org/10.1109/83.366472.
Young, I.M., Crawford, J.W., Rappoldt, C., 2001. New methods and models for characterising structural heterogeneity of soil. Soil Tillage Res. 61, 33–45. https://doi.org/10.1016/S0167-1987(01)00188-X.
Young, I.M., Mooney, S.J., Heck, R.J., Peth, S., 2022. In: 40 years of X-ray CT in soil: Historical context. X-ray imaging of the soil porous architecture. Springer International Publishing. https://doi.org/10.1007/978-3-031-12176-0.
Zagaglia, G., 2012. Sviluppo di un sistema tomografico trasportabile per analisi in situ di reperti paleoantropologici. Tesi di laurea magistrale. Università di Bologna, Bologna, Italia.